Clays and Clay Minerals, Vol. 65, No. 2, 64–91, 2017.

MINERALOGY, GEOCHEMISTRY, AND GENESIS OF BENTONITES IN MIOCENE VOLCANIC-SEDIMENTARY UNITS OF THE ANKARA-ÇANKIRI BASIN, CENTRAL ANATOLIA, TURKEY

Selahattin Kadir[1,*], Tacit Külah[1], Nergis Önalgil[1], Hülya Erkoyun[1], and W. Crawford Elliott[2]

[1] Eskişehir Osmangazi University, Department of Geological Engineering, TR-26480 Eskişehir, Turkey
[2] Department of Geosciences, Georgia State University, Atlanta, GA 30302, USA

Abstract—Widespread alteration in the Miocene lacustrine volcanic/sedimentary rocks of the Ankara-Çankırı basin of central Anatolia has resulted in the formation of sizeable (economic) quantities of bentonite deposits. No detailed characterization of the geological, mineralogical, and geochemical properties or the depositional environments of these primary and secondary bentonite deposits has been carried out to date. The present study was undertaken to close this knowledge gap. Two possible hypothetical processes were examined to explain the genesis of the bentonites: 1) The bentonites were formed by the devitrification of volcanic glass in a lacustrine setting; and 2) The bentonites were formed by the chemical weathering of previously deposited volcaniclastic sediments and ophiolitic materials. The characteristics of the bentonites were examined using X-ray diffractometry, scanning and transmission electron microscopy, energy dispersive spectroscopy, and chemical analyses of major and trace elements. The Ankara-Çankırı bentonites are found gradationally interbedded with parent Miocene volcanic and volcaniclastic rocks. These bentonites were deposited in a shallow lacustrine setting based on observed desiccation cracks, locally enclosed coal seams, plant rootlets, gypsum lenses, yellow sulfate-like fracture infillings, and ferric iron oxide stains. Smectite resulted from the chemical weathering of feldspar and possibly also the weathering of biotite and hornblende. This smectite was precipitated *in situ* on partially dissolved glass and feldspar. The average major-element composition of the smectite-rich clay fractions yielded the following montmorillonitic smectite structural formula: $(Na_{0.33}Ca_{0.31}K_{0.18})(Al_{2.35}Fe_{0.80}Mg_{0.78})(Si_{7.79}Al_{0.21})O_{20}(OH)_4$.

The interlayer cation occupancy in the smectite-rich clay fractions was based on the use of $Na^+/(Na^+{+}Ca^{2+})$ ratios and showed a composition between a Ca-smectite and a Na-smectite. The relative increases in several groups of elements according to the *LREE*/(*MREE*+*HREE)* ratio, Al_2O_3, the sum of Ni+Co+Cr, the sum of Fe_2O_3+MgO+TiO_2, the positive correlation between Rb+Ba and Na_2O+K_2O, Sr and Rb, Rb/Sr and Zr, Zr/Sm and SiO_2, the negative Eu anomaly, and the field and petrographic observations further showed that the Si, Al, Fe, and Mg required to form smectite were mainly supplied from the decomposition of feldspars, amphiboles, and volcanic glass from volcanic materials and were partially supplied from the chemical weathering of ophiolitic basement units. The bentonite deposits examined in this study are mainly primary bentonites derived from volcanics and local secondary bentonites from previously deposited volcaniclastic sediments and ophiolitic materials.

Key Words—Ankara-Çankırı Basin, Bentonite, Genesis, Geochemistry, Mineralogy, Turkey, Volcanics, Weathering.

INTRODUCTION

Smectitic bentonites and K-bentonites are commonly observed in the Phanerozoic Eon (Huff *et al*., 1991; Ver Straeten, 2004; Takagi *et al*., 2005; Środoń *et al*., 2006; Ray *et al*., 2011; Paz *et al*., 2012; Osborn *et al*., 2014; Ekinci Şans *et al*., 2015; Huff, 2016). Only a few occurrences of K-bentonites are known in the Precambrian (*e.g.* Moe *et al*., 1996). Bentonites, as the term is used herein, are argillaceous rocks with a clay mineral fraction that is mostly composed of smectites (and are thus distinguished from K-bentonites). Bentonites are typically formed by the reaction of volcanic materials (glasses or the glassy components of tuff or ash) with lake- or sea-water at the sediment-water interface (*e.g.* Ross and Shannon, 1926; Jeans *et al*., 1982; Christidis and Huff, 2009). While most bentonites are thought to have been formed from volcanic glass at low temperatures, some bentonites are known to have been formed by the hydrothermal alteration of volcanic rocks (Ddani *et al*., 2005; Takagi *et al*., 2005).

The bentonite deposits studied herein are thought to have initially formed by either weathering of volcanic glass or by the weathering of previously deposited volcaniclastic sediments and ophiolitic materials based on the aforementioned studies. Finally, these bentonites comprise a significant bentonite reserve of ~3,000,000 tons (Bakır *et al*., 2012). The bentonites are important sources of raw materials for the drilling, foundry, paper, and bleaching industries in Turkey. The focus of this study is the Miocene bentonite deposits located near

* E-mail address of corresponding author:
skadir.euroclay@gmail.com
DOI: 10.1346/CCMN.2017.064051

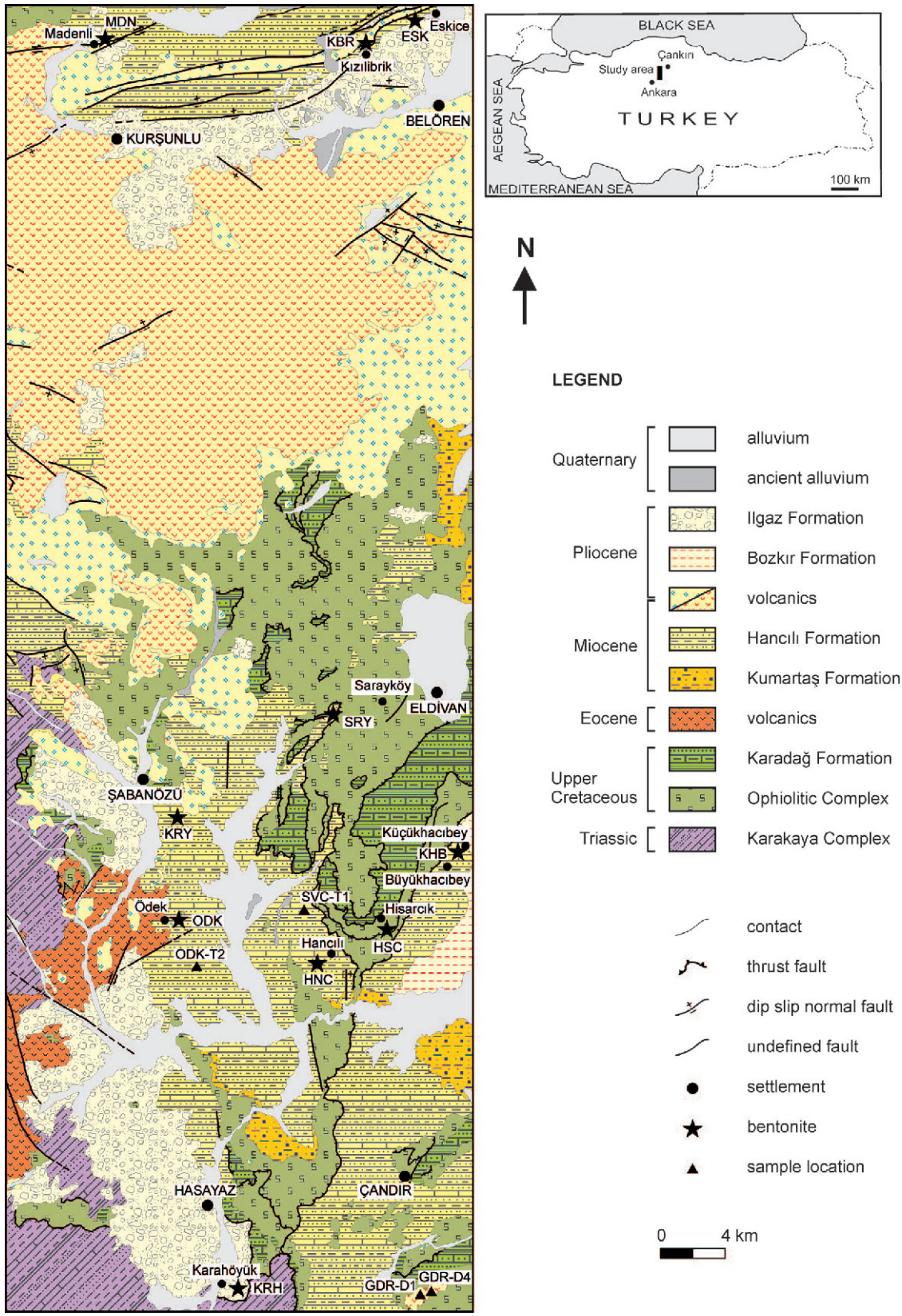

Figure 1. Geological map of the Ankara-Çankırı region (modified from Dönmez and Akçay, 2010; Sevin and Uğuz, 2011).

https://doi.org/10.1346/CCMN.2017.064051 Published online by Cambridge University Press

Kurşunlu, Eldivan, Şabanözü (Çankırı), and Hasayaz (Ankara) within central Anatolia (Figure 1). These bentonites were found between beds of Miocene agglomerate, tuffite, claystone, and marlstone. The Miocene volcanic and sedimentary units lie unconformably above late Cretaceous ophiolitic rocks. To date, the region has been studied for the stratigraphy, geochronology, petrogenesis (Hakyemez *et al.*, 1986; Tüysüz and Dellaloğlu, 1992; Akyürek *et al.*, 1996; Karadenizli *et al.*, 2003; Dilek and Thy, 2006; Gökten and Floyd, 2007), tectonics (Koçyiğit *et al.*, 1995; Okay and Tüysüz, 1999; Kaymakçı, 2000; Seyitoğlu *et al.*, 2000; Göncüoğlu *et al.*, 2006; Dangerfield *et al.*, 2011; Rojay, 2013), mineral compositions, petrography, and clay mineral distributions (Türkmenoğlu *et al.*, 1991; Bakır *et al.*, 2012). There are no detailed studies on the mineralogical, micromorphological, and geochemical characteristics of smectitic bentonites of the Ankara Çankırı basin and the regional depositional environment of the basin, which is the most important source of raw materials in central Anatolia. Two possible hypothetical processes were examined to explain the genesis of the bentonites: (1) the bentonites were formed by the devitrification of volcanic glass in a lacustrine setting; and (2) the bentonites were formed by the chemical weathering of previously deposited volcaniclastic sediments and ophiolitic materials. The main objective of the present study was to fill this knowledge gap and to test these hypotheses through a detailed study of the mineralogy, micromorphology, and geochemistry which should lead to an explanation for the genesis of the bentonites. This study will provide new data and interpretations to determine the physicochemical conditions of the chemical weathering processes and will lead to an understanding of the genesis and early diagenesis of these smectitic bentonites, which have variable amounts of interlayer Ca and Na. Additionally, the depositional conditions that produced the primary and secondary bentonites will be determined based on the lithological, mineralogical, chemical, and climatic changes. These data will guide future exploration and utilization of these bentonite deposits.

GEOLOGICAL SETTING AND DEPOSITIONAL ENVIRONMENT

Geological setting

Basement rocks of the study area comprise the following formations: the Triassic Karakaya Complex, the Upper Cretaceous Karadağ Formation, and the Upper Cretaceous ophiolitic rocks of the İzmir-Ankara-Erzincan Suture Zone (IAESZ). The Triassic Karakaya Complex is composed of arkosic sandstone, greywacke, mudstone, and conglomerate. The Upper Cretaceous Karadağ Formation is composed of clayey-silty limestone, sandstone, and mudstone. The IAESZ comprises a complex assemblage of serpentinized ultramafic rocks, gabbro, diabase, plagioclase-rich granite, spilite, spilitic basalt, basic dikes, radiolarite, mudstone, and pelagic limestone (Sevin and Uğuz, 2011; Figures 1–3).

Various types of Eocene volcanic rocks unconformably overlie the basement rocks of the study area (Figures 1, 2). These Eocene rocks include dacite, rhyolite, perlite, basalt, and pyroclastics and are overlain unconformably by the Miocene Kumartaş Formation. The Kumartaş Formation consists of conglomerate, sandstone, and siltstone. The Miocene Hancılı Formation consists mostly of alternating sandstone, siltstone, and argillaceous limestone with interbeds of conglomerate, tuffite, bituminous shale, coal bands, and gypsum. The Kumartaş Formation and Hancılı Formation have lateral and vertical transitions between the two formations. Lacustrine deposits of the Hancılı Formation also have lateral and vertical transitions with the Miocene-Pliocene lava flows and pyroclastic rocks. The volcanic rocks range in composition from basalt, andesite, and dacite to rhyolite. The Pliocene Ilgaz Formation consists of conglomerate, sandstone, and mudstone and discordantly overlies the older units. The Ilgaz Formation has lateral and vertical transitions with the Pliocene Bozkır Formation, which is composed of gypsum, sandstone, mudstone, and tuffite. All the aforementioned rocks are overlain unconformably by Quaternary alluvium.

Lithology

The following lithologies have been distinguished within the Miocene sediments in the study area and are described below.

Conglomerate. This conglomerate consists of pebbles, cobbles, and fragments of ophiolites and sedimentary rock in a friable yellowish-gray matrix. The fragments were weathered from the basement rocks. The pebbles and cobbles are well rounded to sub-rounded, are unsorted, and vary from a few cm to 50 cm in diameter. The conglomerates are mainly matrix supported and the matrix consists of sandy, silty, and argillaceous materials (Figure 3a).

Sandstone. This sandstone facies is composed of yellowish gray, medium- to coarse-grained, fine- to medium-bedded, polygenetic sandstones. The sandstones contain local occurrences of carbonate and clay matrix (Figure 3b).

Mudstone. This mudstone facies is characterized by alternation of mudstone layers with different colors and thicknesses (green-gray, yellow-brown, yellow, brown, and reddish-brown) (Figures 3a, 3b). The mudstones contain recent desiccation cracks and relict plant rootlets. The mudstones are locally rich in organic material and include coal, carbonate, and veins, bands, and lenses of gypsum (Figures 3c–3e).

https://doi.org/10.1346/CCMN.2017.064051 Published online by Cambridge University Press

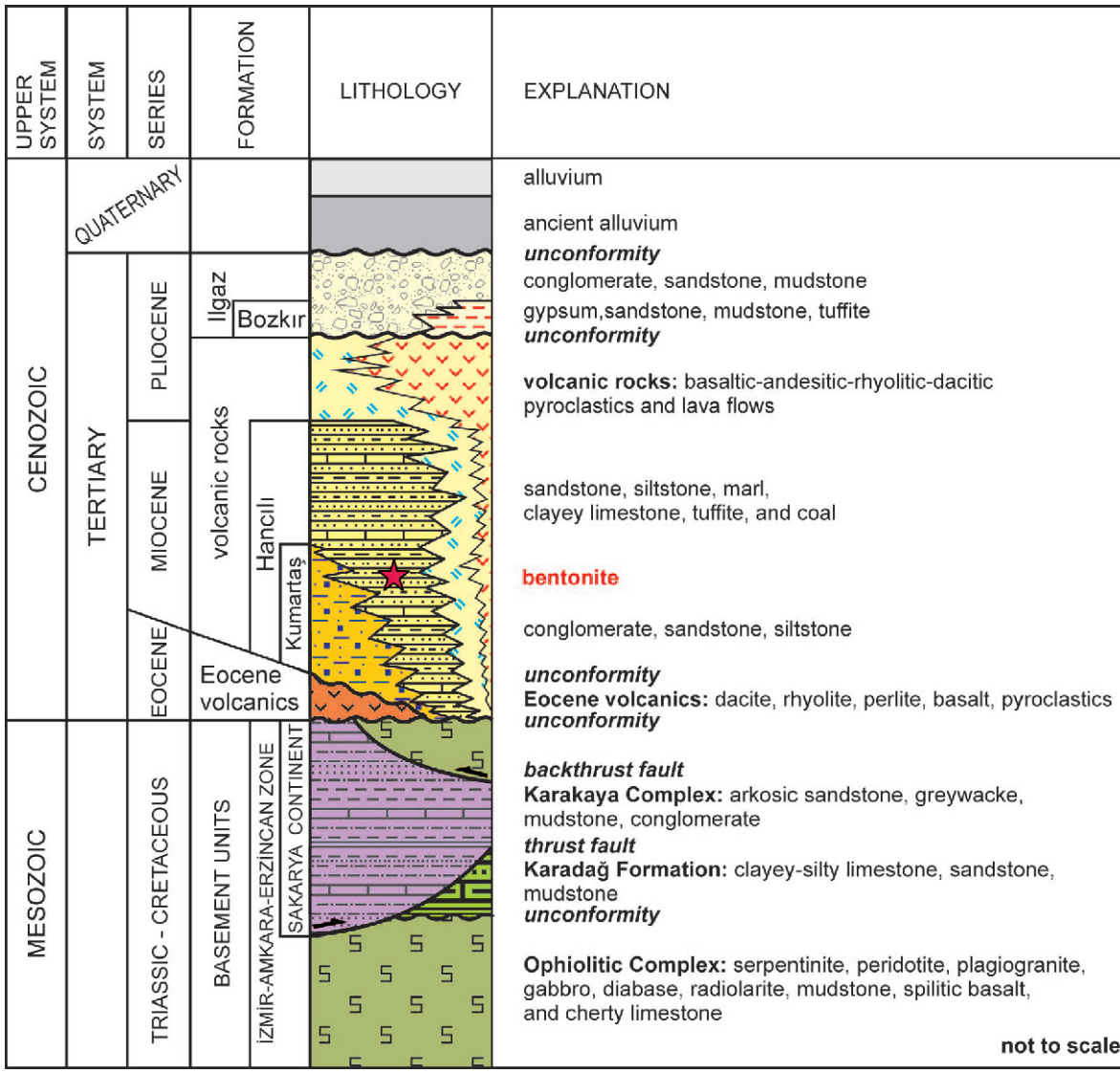

Figure 2. Stratigraphic section of the study area (modified from Sevin and Uğuz, 2011). Stratigraphic symbols defined in Figure 1.

Limestone. This limestone is cream in color, thin-bedded, and contains local occurrences of argillaceous limestone (Figure 3d).

Coal. This facies is represented by dark brown and black coal levels within mudstones and the coal levels vary from a few cm to 50 cm thick (Figure 3d).

Tuffite. This tuffite facies is friable and thin-bedded. It is composed of reworked epiclastic rock fragments and volcanic materials, such as pumice, volcaniclastic grains, and devitrified glass shards. It is white, gray, or pinkish-white in color. The composition of the tuffite ranges from dacitic to rhyolitic, but it is mainly andesitic and the tuffaceous units show argillization (Figure 3f).

Description of bentonite deposits

Bentonites of the Ankara-Çankırı basin and the bentonites outside the basin with igneous and sedimentary rocks were collected from ten known bentonite deposits within the Hancılı Formation. The bentonite deposits are described below by name and descriptions, beginning with the bentonites in the north of the study area and progressing southward (Figures 3, 4).

Eskice Deposit (ESK). This deposit lies above a fossiliferous and sandy limestone and alternates with a claystone that comprises the base of the Hancılı Formation. A grayish-green and grayish-white bentonite that exhibits recent desiccation cracks and popcorn-shapes on the surfaces are found above the basal limestones and claystones. The total thickness of the

https://doi.org/10.1346/CCMN.2017.064051 Published online by Cambridge University Press

Figure 3. Field photographs of the Ankara-Çankırı bentonite deposits: (a) conglomerate and mudstone in the bentonite deposits (Eskice deposit); (b) alternation of mudstone and sandstone in the Karahöyük bentonite deposit (KRH-7); (c) close-up view of bentonite in Küçükhacıbey deposit (KHB-10); (d) argillaceous limestone and coal in bentonite beds (Madenli deposit); (e) close view of gypsum lens within Karahöyük bentonite (KRH-3); (f) tuffite units that host Eskice bentonite deposit in the Karahöyük (KRH-9); (g) general views of the Küçükhacıbey.

https://doi.org/10.1346/CCMN.2017.064051 Published online by Cambridge University Press

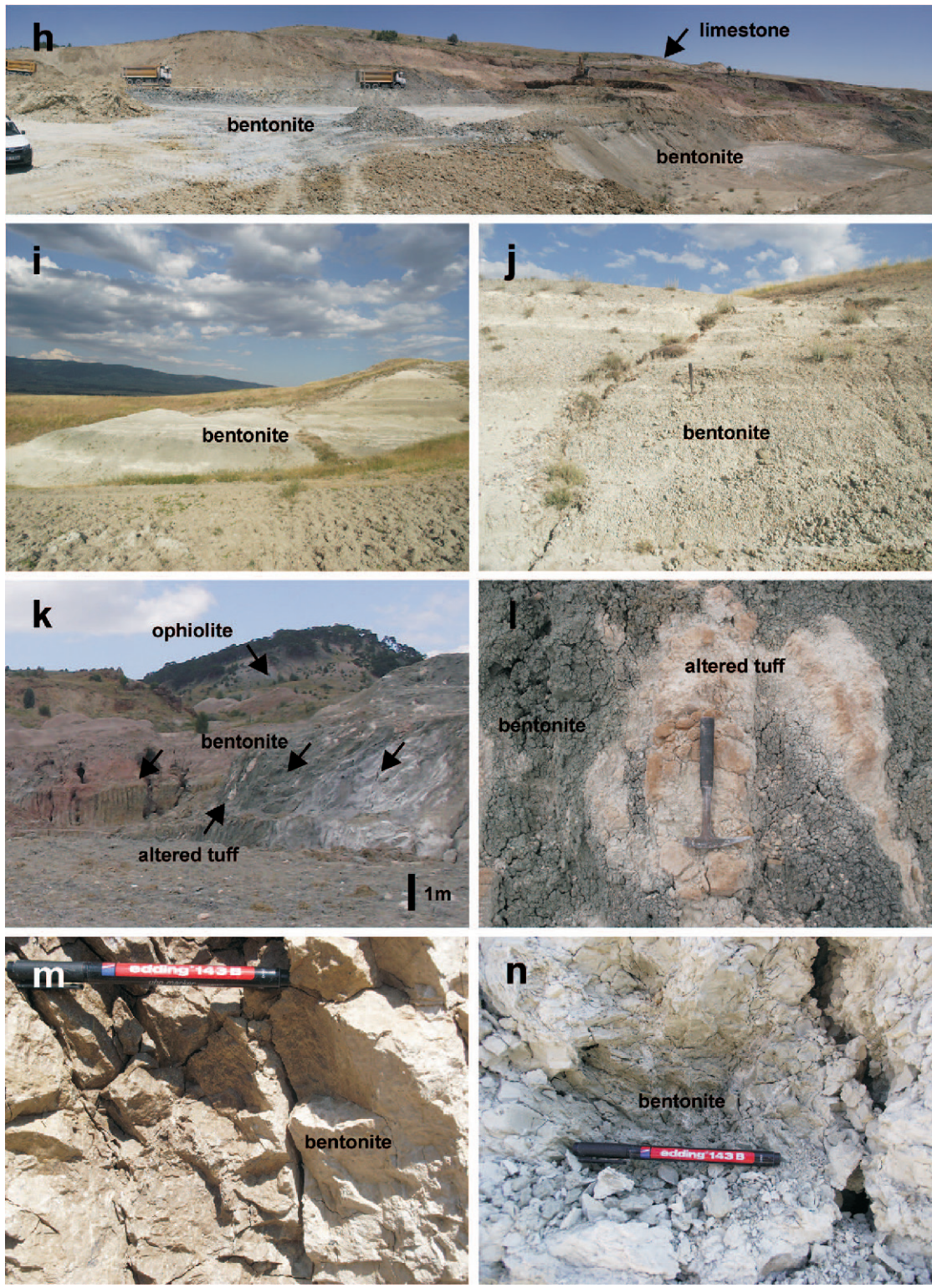

Figure 3 (*contd*.). Field photographs of the Ankara-Çankırı bentonite deposits: (h – j) general views of the Hancılı (h) and Ödek (i, j) bentonite deposits; (k) tuffaceous lenses between bentonite layers in the Küçükhacıbey bentonite deposit, overlain by ophiolitic units (KHB-8); (l) relict of tuffaceous material in Küçükhacıbey bentonite deposit (KHB-8); (m,n) close-up view of bentonite from Karayatak and Hancılı deposits (KRY-5, HNC-2).

https://doi.org/10.1346/CCMN.2017.064051 Published online by Cambridge University Press

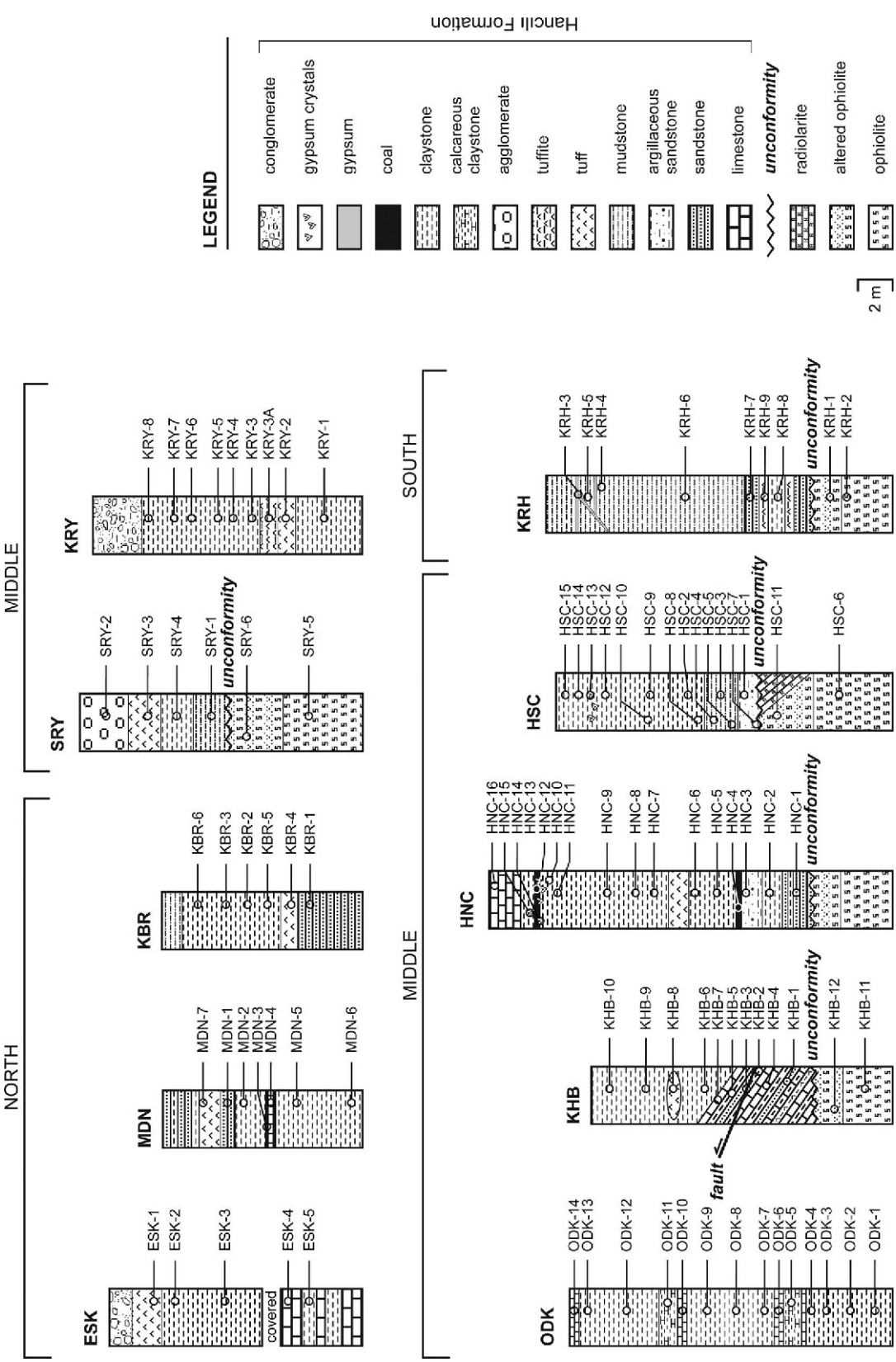

Figure 4. The distribution of the principal lithologies in the Ankara-Çankırı bentonite deposits. See Figure 1 for section locations and Table 1 for the mineralogical compositions of selected samples.

https://doi.org/10.1346/CCMN.2017.064051 Published online by Cambridge University Press

bentonite in this section is ~8 m. This bentonitic deposit is covered by a purple-gray tuffite and a conglomerate. The deposit constitutes a probable Ca-bentonite reserve of 1,400,000 tons (Bakır *et al.*, 2012) and is currently being mined to supply the foundry, drilling, and food industries.

Madenli Deposit (MDN). This deposit starts at the lower contact as a dark green and green bentonite and exhibits conchoidal fracture, recently formed desiccation cracks, and popcorn-form surfaces. The total thickness of this Ca-bentonite is ~7 m and the upper beds of this bentonite interfinger with thin lenses of coal and limestone. The interfingered coal and limestone beds are covered by tuffaceous sandstones and tuff. This deposit contains an appreciable tonnage of Ca-bentonite and is mined for the drilling and foundry industries, but the reserve quantity has not been calculated (Bakır *et al.*, 2012).

Kızılibrik Deposit (KBR). A grayish-white bentonite that overlies purple to gray basal sandstones and locally contains gravel and grayish-white tuffs of the Hancılı Formation. This bentonite has recent desiccation cracks, a popcorn-form, a total thickness of ~8 m, and was previously discovered and mined (Bakır *et al.*, 2012).

Saray Deposit (SRY). Dark green, fractured, and highly serpentinized ophiolitic rocks are overlain by a mudstone and a brownish-white silty and sandy bentonite with a popcorn-form. This sandy bentonite continues upward and changes into a light brown to cream color bentonite. The thickness of each bentonite is ~2.5 m and are overlain by pinkish-brown pumice tuff and pinkish-brown agglomerate. This bentonite is used in foundry, paper production, and drilling, but is not suitable for the ceramic industries and the reserve of this deposit has not been calculated (Bakır *et al.*, 2012).

Karayatak Deposit (KRY). This deposit contains a basal dark-green, friable, and locally iron-oxidized bentonite with a thickness of ~4 m. This dark green bentonite progressively changes upward into a massive, beige-colored bentonite, an iron-oxidized tuff, a light green pumice, and finally a sandy tuffite. The uppermost reddish brown, plastic, bentonite (~8 m thick) has recent desiccation cracks (Figure 3m) and is covered by reddish-brown conglomerates. When the major element composition is used to calculate a smectite formula, the interlayer composition of the calculated formula contains significant amounts of both Na and Ca. The Karayatak bentonites are mined as foundry clays and the deposit has a probable reserve of 150,000 tons (Bakır *et al.*, 2012).

Ödek Deposit (ODK). This deposit contains dark green, cream, and dark gray bentonites. The bentonite alternates with a cream- to beige-colored claystone with calcareous claystone beds and thin limestone laminations, and it directly overlies the ophiolitic basement. Total thickness of the bentonite is ~15 m, the deposit is covered by cream- to beige-colored limestone beds that are 25–30 cm thick (Figure 3i, 3j), but the mine is now closed (Bakır *et al.*, 2012).

Küçükhacıbey Deposit (KHB). This deposit alternately consists of limestone, mudstone, sandstone, and tuffite of the Hancılı Formation and the sediments discordantly overlie the ophiolitic basement rocks (Figures 3k, 3l). A green colored bentonite overlies these basal sediments and has recent desiccation cracks and a popcorn-form. This bentonite continues upward as a reddish-brown bentonite with a thickness of ~7 m and a total thickness in this section of ~9 m (Figure 3g). This bentonite has a Na composition, is mined for use in the drilling and foundry industries, and has a reserve of 288,000 tons (Bakır *et al.*, 2012).

Hancılı Deposit (HNC). A basal ophiolitic unit is overlain unconformably by greenish-gray, clayey, tuffaceous sandstone of the Hancılı Formation. This clayey sandstone continues upward to become a gray and greenish-gray, plastic bentonite with recent desiccation cracks (Figure 3n). This bentonite encloses a 30-cm thick coal band and is overlain by a gray tuff. Above the gray tuff, the bentonite continues upward with white, gray, yellowish-brown, and brown colored beds. The uppermost beds contain gypsum lenses and a coal. Total thickness of the bentonite is ~12 m. The gypsum and coal beds are overlain by white to cream-colored limestone. As in the KRY bentonite, the interlayer composition of this smectite contains both Na and Ca and the deposit is mined for the paper, drilling, and foundry industries, and has a reserve of 760,000 tons (Bakır *et al.*, 2012).

Hisarcık Deposit (HSC). Ophiolitic rocks, including radiolarite, are overlain unconformably by a grayish-green, argillaceous sandstone with ophiolitic pebbles. This sandstone changes into a mudstone and a yellowish-green, plastic, dark brown, brownish-green, green, and reddish-brown bentonite. The upper beds of this bentonite enclose gypsum crystals as large as a few centimeters. Total thickness of the bentonite is ~8 m, the one mine from this deposit is no longer active, and approximately 324,000 tons of bentonite were mined for foundry clays from this deposit (Bakır *et al.*, 2012).

Karahöyük Deposit (KRH). White-gray, yellow, and brownish red bentonites are found stratigraphically above underlying deposits of the Hancılı Formation that alternate between sandstone, mudstone, and tuffite and unconformably overlie the ophiolitic rocks of the basement. The uppermost bentonite is crosscut by gypsum veins a few cm thick. This bentonite also

https://doi.org/10.1346/CCMN.2017.064051 Published online by Cambridge University Press

encloses sub-rounded to rounded and abundant terrigenous materials and ophiolitic clasts with grain sizes that range from a few mm to a few cm with concentrations of ~20% and the clasts resemble reworked pyroclastic units. Total thickness of the bentonite is ~14 m, the deposit is currently used for drilling and foundry clays, and it has a probable reserve of 40,000 tons (Bakır *et al.*, 2012).

MATERIALS AND METHODS

Field work was carried out using existing geological maps of the Çankırı region (Dönmez and Akçay, 2010; Sevin and Uğuz, 2011) to identify the lateral and vertical distribution of bentonites and the host rocks within the Miocene lacustrine volcanic-sedimentary units of the study area. Up to 500 g of sample was collected from each bentonite bed in these sections (Figure 4). Optical microscope studies were carried out on fresh and partially altered tuff, tuffite, and dacite. Samples selected to represent various degrees of alteration were manually crushed and powdered using a tungsten carbide pulveriser for X-ray diffraction (XRD) and geochemical analyses.

Separation was undertaken following the removal of iron(III) oxide cements, carbonate cements, and organic matter (Kunze and Dixon, 1986). The treated samples were sieved to <2 mm and 100 g of the <2 mm fraction was mixed with deionized water and disaggregated using a 'Stir-Pak' (Cole-Parmer, Vernon Hills, Illinois, USA) mixer head and mixer controller. The <2 μm fractions were separated from the silt (2-50 μm) by using repeated siphoning of the dispersed material. The clay fraction was separated by sedimentation of the suspension after 24 h dispersion in distilled water and removal of the upper 5 cm, followed by centrifugation for 10 min at 4000 rpm using a Hettich 32A centrifuge (Andreas Hettich GmbH & Co. KG, Tuttlingen, Germany).

The mineralogical characteristics of the samples were determined using powder X-ray diffractometry (XRD) (Rigaku D/Max−2200, Ultima PC, Tokyo, Japan). The bulk powders and clay mounts were scanned using CuKα radiation (40 kV and 30 mA) with a 1º divergence slit, a 0.15º antiscatter slit, and a 1º receiving slit. A 0.30 mm monochromator receiving slit and monochromator were used to filter out all but CuKα radiation. The samples were scanned at a speed of 1º2θ/min. Random mounts of powdered samples were scanned to determine the mineralogy of bulk samples. Semi-quantiative mineral analyses were determined from random mounts of the whole rock powders using a PANalytical X'Pert Pro X-ray diffractometer (PANalytical, Almelo, The Netherlands) at Georgia State University. Random mounts were produced using the backfill method (Moore and Reynolds, 1997). The random mounts were scanned using Ni-filtered Cu radiation produced at 45 kV and 40 Ma using a 1º divergence slit, a 2º antiscatter slit, and a 1º receiving slit. The mounts were scanned at 1º2θ per minute from 2 to 65º2θ. The High Score™ program was used to estimate semi-quantitative mineral compositions using the knowledge gained from the diffraction analysis of the bulk powders.

Several oriented mounts were prepared from each clay fraction by dropping a small amount of clay suspension onto a glass slide and drying in air. One oriented mount was solvated using ethylene glycol vapor at 60ºC for 2 h to expand and identify smectites. Other oriented mounts were heated at 300ºC and at 550ºC for 2 h to identify chlorite and kaolinite. Bulk samples that contained large amounts of smectite were treated prior to size separations to remove carbonate cements, organic matter, and iron(III) oxide cements before chemical analyses (Kunze and Dixon, 1986).

Scanning electron microscopy (SEM) studies were performed at Anadolu University (Turkey) using a Zeiss Supra™ 50 VP field emission (FE-SEM) instrument (Carl Zeiss AG, Jena, Germany) equipped with an energy-dispersive X-ray (EDX) spectrometer.

The bulk specimens that were dominantly clay were prepared for SEM-EDX analyses by sticking the freshly broken surface of each rock sample onto an aluminum sample holder using double-sided tape. The samples were then coated with a thin film (~350 Å) of gold using a Giko IB-3 ion coater (Giko Engineering Co. Ltd., Japan). Transmission electron microscopy (TEM) studies were carried out at Bilkent University (Ankara, Turkey) using a FEI Tecnai F30™ (FEI/Thermo Fisher Scientific, Hillsboro, Oregon, USA) instrument. The clay particles for TEM analysis were dispersed in an ultrasonic ethanol bath for ~30 min and one drop of each clay suspension was placed on a carbon-coated copper grid and dried at room temperature.

Fourteen bentonites, 5 tuffs/tuffites, and 2 dacites were analyzed for major and trace elements at the Bureau Veritas Mineral Laboratories (Vancouver, Canada) using a PerkinElmer Elan 9000 (PerkinElmer, Inc., Waltham, Massachusetts, USA) inductively coupled plasma−atomic emission spectrometer (ICP-ES) and mass spectrometer (ICP-MS) and a Spectro (Spectro Analytical Instruments Inc., Mahwah, New Jersey, USA) XLAB-2000 PEDX-ray fluorescence spectrometer (PEDXRF), which was calibrated using USGS interlaboratory standards. The ICP-ES and ICP-MS analyses were carried out on lithium metaborate/tetraborate fused samples after dissolution in dilute nitric acid. Loss on ignition (LOI) values were determined from the mass differences before and after ignition at 1000ºC. Total Fe was reported as Fe_2O_3 and total C was determined by ignition followed by measurement by an infrared spectrometric cell in a LECO Carbon Analyzer (LECO Corporation, Saint Joseph, Michigan, USA) by Bureau Veritas, Vancouver, Canada.

The detection limits for the chemical analyses were 0.01 wt.% for most major element oxides, but was

https://doi.org/10.1346/CCMN.2017.064051 Published online by Cambridge University Press

0.002 wt.% for Cr_2O_3, 0.04 wt.% for Fe_2O_3, 0.02 wt.% for total C and total S, 0.1 wt.% for LOI, and between 0.01 and 1 mg/kg for almost all trace elements. Samples were analyzed in duplicate and the accuracy and analytical precision of the major element measurements were assessed by analyzing the standard reference materials STD SO-18, STD SO-19, STD GS311-1, and STD GS910-4 for major elements and by analyzing the standard reference materials STD SO-18, STD SO-19, STD DS10, and STD OREAS45EA for trace elements.

Fresh andesitic, borehole core samples with an average Zr/TiO_2 ratio of ~0.03 were collected from a 14–29.5 m depth in the host rock of the Hancılı bentonite deposit (Aker, 2013). The bentonite, which has an average Zr/TiO_2 ratio of ~0.02, was used as a reference for mass gain and loss calculations. Mass gains and losses have been estimated by using the EASYGRESGRANT program (López-Moro, 2012) and from plots of the geochemical analyses on isocon diagrams (Grant, 1986, 2005):

$$C_i^A = (M^O/M^A)C_i^O$$

where C_i is the concentration of component i, O indicates the fresh rock, and A indicates the altered rock. The M^O and M^A values are the equilibrium masses (as wt.% or ppm) of the fresh and altered rocks, respectively.

The C_i^A/C_i^O ratios were plotted to obtain the slopes of the isocon graphic lines from the fresh and the altered rock analytical data using the following equation:

$$\Delta C_i/C_i^O = (M^O/M^A)(C_i^A/C_i^O) - 1$$

where ΔC_i is the gain or loss of mass. MgO and Rb were assumed to be immobile based on clusters of slopes that were close to 1.00.

If a constant mass is assumed,

$$\Delta C_i/C_i^O = (C_i^A/C_i^O) - 1$$

Thus, sample compositions that plot above the isocon line indicate a gain during the alteration process and samples that plot below this line represent a loss during alteration.

The structural formulas of smectites were determined for the <2 μm clay fraction of samples with the largest smectite content as indicated by XRD. The structural formulas of the bentonite smectites were calculated on the basis of 22 oxygen atoms (Newman and Brown, 1987). The tetrahedral sites of smectite were filled with Si and Al as needed to produce a sum of eight atoms. The remaining Al and the Fe and Mg were assigned to octahedral sites. All Fe was reported as Fe(III) in the chemical analyses. The Ca, Na, and K in the chemical analyses were allocated as exchangeable interlayer cations.

RESULTS

Petrography

The andesitic tuffs/tuffites and dacite occur within and beneath the Ankara-Çankırı bentonites (Figures 5a–5f) and these rocks have a porphyritic texture. The primary minerals are K-feldspar (orthoclase) with Carlsbad twinning, plagioclase (andesine), biotite, prismatic hornblende, some opaque minerals, and rock fragments in a fine-grained matrix with volcanic glass (Figures 5a–5d). The tuffitic rocks are characterized by the presence of approximately 30% subrounded volcanic and ophiolitic fragments with a grain size that ranges from 0.42 to 0.84 mm in a volcanic groundmass (Figures 5e, 5f). The K-feldspar and plagioclase have been partially to completely transformed into clay (Figures 5a–5c, 5g, 5h). Biotite and hornblende have been partially to completely oxidized to Fe(III) oxides (Figures 5a–5d, 5g, 5h). Devitrified glass and locally reddish-brown Fe oxide stains are abundant in the volcanic groundmass as indicated by petrographic examination.

The partially altered dacites, that were located close to the bentonite deposits, were originally composed of plagioclase (oligoclase/andesine), K-feldspar (sanidine), hornblende, biotite, and quartz phenocrysts. These silicate phases exhibit a porphyritic texture cemented by devitrified volcanic glass (Figures 5g, 5h).

XRD determinations

The XRD analyses of the bulk samples of the bentonite, tuffaceous units, and the clay fractions are given in Table 1 and in Figure 6. Smectite was the most abundant alteration product in these bentonite deposits, but chlorite and illite were found in some of these bentonite/tuffs. Smaller amounts of quartz, feldspar, dolomite, calcite, and opal-CT were found in the clay fractions. Minor amounts of clinoptilolite (sample KRH-9, tuffite) and analcime (sample KHB-7, dolomite) were observed (Table 1). The smectite amounts were higher in the bentonite deposits in both the north (Eskice, Madenli, Kızılibrik) and the middle part of the study area (Karayatak, Küçükhacıbey, Hancılı, Hisarcık except Ödek) relative to the smectite amounts in the southern bentonite deposit (Karahöyük). Smectite had a variable lateral and vertical distribution and the illite and chlorite contents increased south of the basin (Table 1).

The smectite had sharp basal reflections with d_{001} values that varied between 14.12–14.87 Å and 12.67 Å. These diffraction peaks expanded to 16.66–17.06 Å after solvation with ethylene glycol. The peaks collapsed to 9.41–9.88 Å after heating the oriented mounts at 300ºC for 2 h and collapsed to 9.53–9.93 Å after heating at 550ºC, respectively (Figure 6). The d_{060} of the smectite was 1.50 Å and suggests a dioctahedral character (Moore and Reynolds, 1989). The Ca-smectite and Na-smectite were identified based on the d_{001}

https://doi.org/10.1346/CCMN.2017.064051 Published online by Cambridge University Press

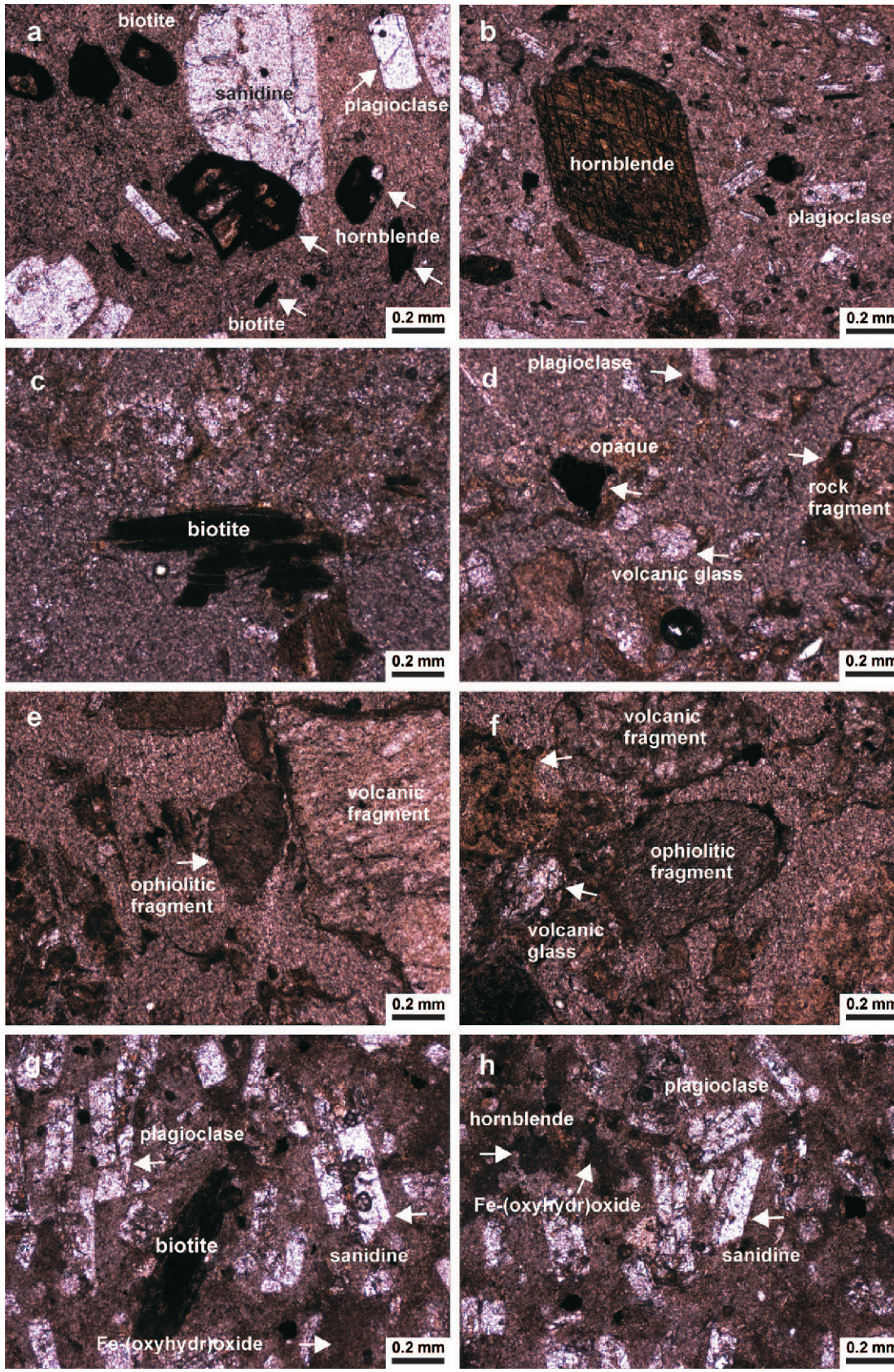

https://doi.org/10.1346/CCMN.2017.064051 Published online by Cambridge University Press

Table 1. Semi-quantitative mineralogical compositions of the bentonite and volcanic host rock samples. Note the following mineral abbreviations were used: An (anorthite), Ab (albite), Tr (trace), Sme (smectite), Ilt (illite), Chl (chlorite), Fsp (feldspar), Qz (quartz), Opl (opal-CT), Cal (calcite), Dol (dolomite), Cpt (clinoptilolite), Anl (analcime) (mineral name abbreviations after Whitney and Evans, 2010).

Sample	Rock type	Sme	Ilt	Chl	Fsp	Qz	Opl	Cal	Dol	Cpt	Anl
North											
Eskice											
ESK-3	Bentonite	50	23			13		6	8		
Madenli											
MDN-5	Bentonite	56				9		35			
Kızılibrik											
KBR-3	Bentonite	77				23					
KBR-5	Bentonite	66			16(An)	16					
KBR-6	Bentonite	42	10			15		33			
Middle											
Karayatak											
KRY-3	Bentonite	85			11(Ab)	3	1				
KRY-5	Bentonite	57			43						
Ödek											
ODK-1	Bentonite	22	14	13	19(An)	19			13		
ODK-2	Bentonite	41	14			28			16		
ODK-9	Bentonite	30	14	18	Tr(An)	18			20		
ODK-12	Bentonite	32	8	21		12			23		
Küçükhacıbey											
KHB-7	Dolomite					5			77		11
KHB-9	Bentonite	72	24			2			4		
Hancılı											
HNC-6	Bentonite	66				27	7				
HNC-7	Bentonite	85	8		4(An)	3					
HNC-8	Bentonite	82				16	2				
Hisarcık											
HSC-12	Bentonite	53		35	5(An)	4	2				
HSC-15	Bentonite	47		44		9	1				
South											
Karahöyük											
KRH-4	Bentonite	33	26	20		20					
KRH-6	Bentonite	39	9			42					
KRH-9	Tuffite				55(An)	30				15	

reflections observed at 14.12–14.87 Å and 12.67 Å, respectively. Ethylene glycol treatment and heat treatment had almost no effect on the d_{001} reflection at 14.12 Å (*i.e.* chlorite). Chlorite was identified from diffraction peaks at 14.12 Å, 7.05–7.06 Å, and 3.53 Å. Small amounts of plagioclase feldspar were defined from diffraction peaks at 3.16–3.22 Å. The presence of accessory illite was determined by peaks at 9.93–9.95 Å and 4.97–5.01 Å (Figure 6). Gypsum, calcite, and dolomite were identified based on the characteristic diffraction peaks at 7.58 Å, 3.03 Å, and 2.88 Å, respectively (Figure 6).

SEM-EDX and TEM analyses

The SEM images indicated that smectite occurs as massive micron-sized flakes in the bentonites (Figures

Figure 5 (*facing page*). Photomicrographs of (a–c) altered feldspar and oxyhornblende and oxybiotite in tuff viewed in plane-polarized light (KBR-4); (d) altered plagioclase, rock fragment, volcanic glass, and opaque-mineral bearing tuffite viewed in plane-polarized light (KRH-9); (e,f) volcanic and ophiolitic fragments in groundmass of tuffite viewed in plane-polarized light (KRY-3A); (g,h) Fe-(oxyhydr)oxidized biotite, hornblende, and argillized plagioclase and sanidine in groundmass of dacite viewed in plane-polarized light (GDR-D1).

https://doi.org/10.1346/CCMN.2017.064051 Published online by Cambridge University Press

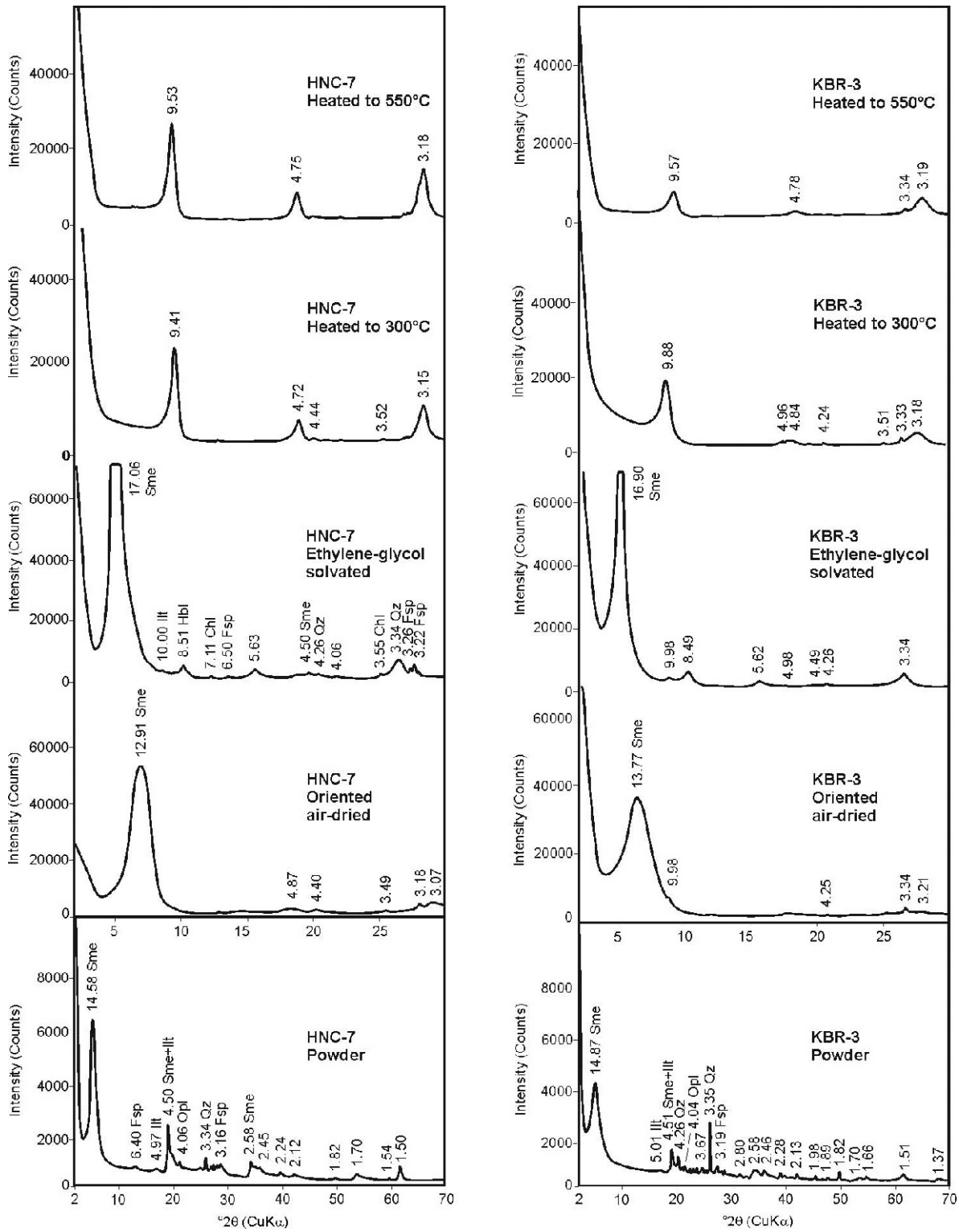

Figure 6. X-ray diffraction patterns of the bentonite samples in the Ankara-Çankırı Areas: HNC-7 and KBR-3 powder, oriented air-dried, ethylene glycol solvated, heated to 300ºC, and heated to 550ºC. Sme: smectite; Ilt: illite; Chl: chlorite; Fsp: feldspar; Qz: quartz; Opl: opal-CT; Cal: calcite; Dol: dolomite; Gp: gypsum; Hbl: hornblende (mineral name abbreviations after Whitney and Evans, 2010).

https://doi.org/10.1346/CCMN.2017.064051 Published online by Cambridge University Press

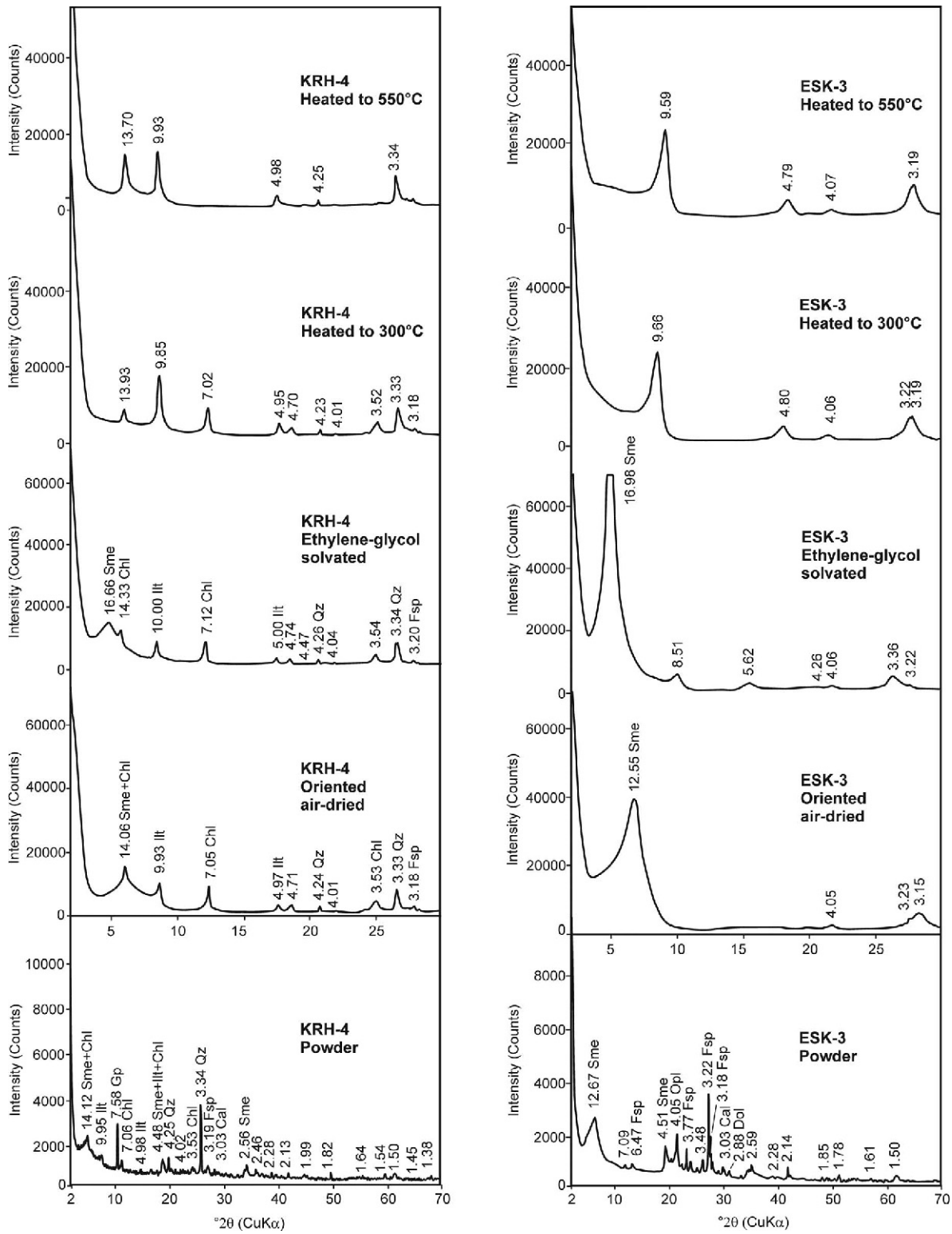

Figure 6 (*contd.*). X-ray diffraction patterns of the bentonite samples in the Ankara-Çankırı Areas: KRH-4 and ESK-3 powder, oriented air-dried, ethylene glycol solvated, heated to 300ºC, and heated to 550ºC. Sme: smectite; Ilt: illite; Chl: chlorite; Fsp: feldspar; Qz: quartz; Opl: opal-CT; Cal: calcite; Dol: dolomite; Gp: gypsum; (mineral name abbreviations after Whitney and Evans, 2010).

https://doi.org/10.1346/CCMN.2017.064051 Published online by Cambridge University Press

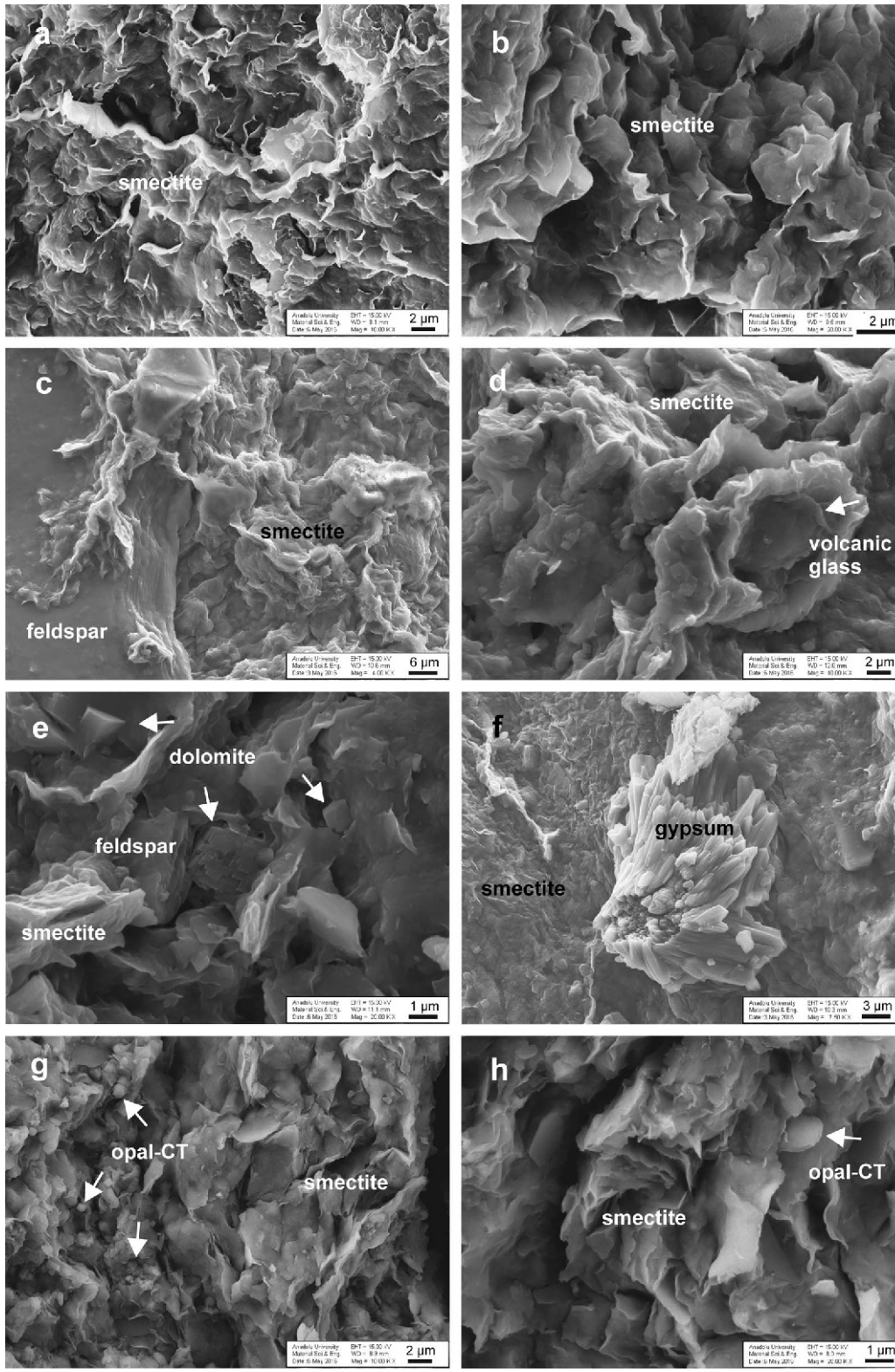

Figure 7. SEM images showing: (a) flaky smectite (HSC-8); (b) close-up view of smectite flake in (a); (c) close-up view of smectite edge with degraded feldspar grain (KRY-5); (d) smectite enclosing devitrified volcanic glass particle (ODK-2); (e) euhedral dolomite crystals in pores between smectite flakes enclosing a feldspar grain (ODK-2); (f) gypsum rosette covering smectitic materials (HNC-7); (g,h) rounded particles in pore between smectite flakes that resembles opal-CT (KRH-6).

https://doi.org/10.1346/CCMN.2017.064051 Published online by Cambridge University Press

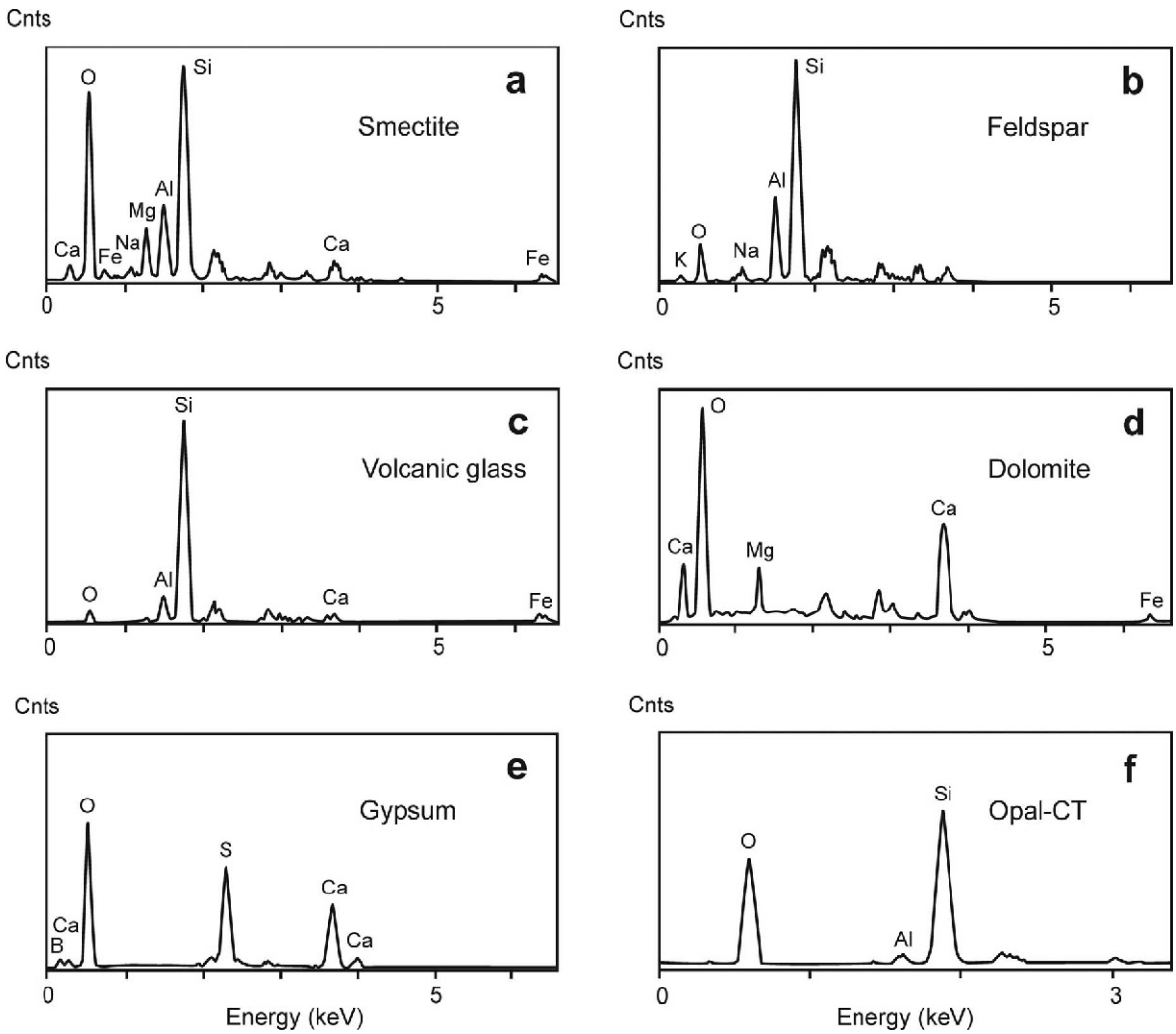

Figure 8. EDX analyses of: (a) smectite; (b) feldspar; (c) volcanic glass; (d) dolomite; (e) gypsum; and (f) opal-CT.

7a, 7b, 8a). These smectite flakes were mostly found between grains or enclosing relict feldspar and volcanic glass grains (Figures 7c, 7d, 8b, 8c). The smectite flakes had diameters between 0.3 and 3 μm and had locally irregular outlines and edges. The smectite flakes suggest formation *via* a dissolution-precipitation mechanism (Chamley, 1989; Vitali *et al.*, 1999; Kadir *et al.*, 2014). This suggestion was also supported by the development of a dull-white gel-like material between smectite and volcanogenic grain boundaries (Figures 7c, 7d).

Pores between the smectite flakes enclose euhedral micritic dolomite crystals with 0.2–0.8 μm diameters (Figures 7e, 8d). These dolomite grains were interpreted to have formed authigenically. Furthermore, the presence of Ca^{2+} and SO_4^{2-} in the pore water resulted in the precipitation of prismatic laths of gypsum arranged as rosettes (Figures 7f, 8e). The gypsum laths had 1.5–7 μm lengths and 1–1.5 μm widths. Rounded particles of opal-CT with diameters of 1.5–2 μm were identified, some in dissolution voids (Figures 7g, 7h, 8f).

TEM analyses also revealed that the smectite exhibits platy forms with regular outlines (Figures 9a, 9b) and dimensions of 0.4 to 1 μm.

Chemical analyses

The concentrations of the major elements varied among the bentonites. For example, the average Al_2O_3 content for the bentonites of the study area varied from 12.73 to 20.56 wt.%. The average Fe_2O_3 content from the sections varied from 4.22 to 8.38 wt.%. The average SiO_2 concentration varied from 45.48 to 50.87 wt.%. The average MgO content ranged from 1.97 to 3.70 wt.%. The average K_2O content ranged from 1.32 to 2.81 wt.%. The average LOI value ranged from 13.50 to 18.77 wt.%. The amounts of the major elements reflect the overall smectitic mineralogy of these samples (Tables 1, 2). Please see extended version of Table 2, Table S1 in the

https://doi.org/10.1346/CCMN.2017.064051 Published online by Cambridge University Press

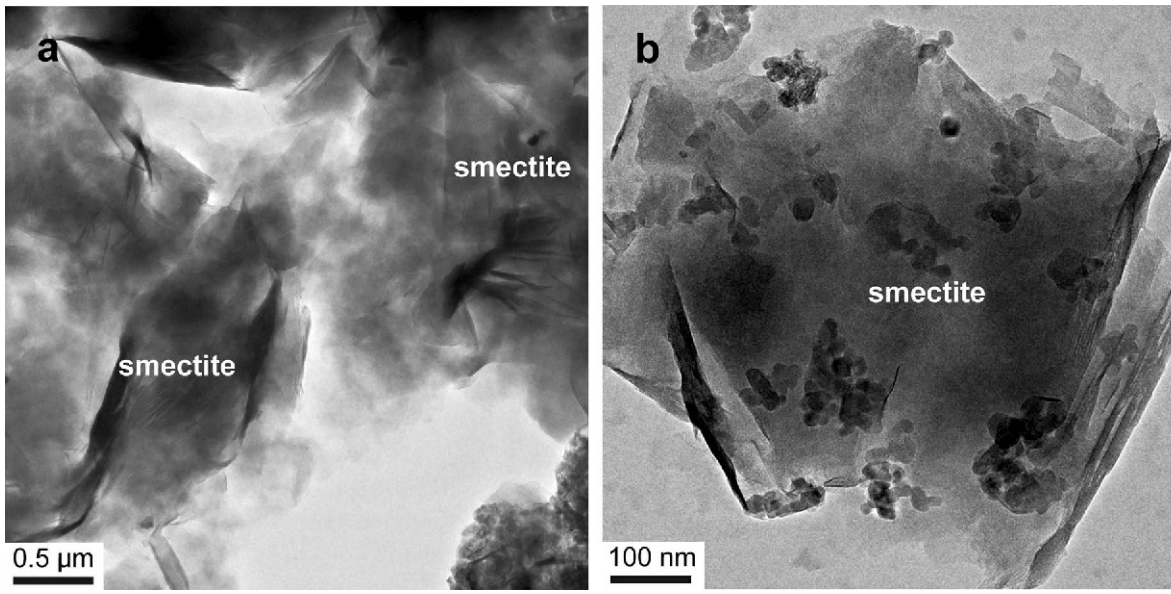

Figure 9. TEM images of: (a, b) smectite flakes (HNC-7; HSC-8).

Table 2. Average major oxide (wt.%), minor element, and trace element (ppm) contents of the bentonite, tuff/tuffite, dacite, and tuff/andesite in the study area.

Major oxides (wt.%)	Bentonite North Avg. (n = 3)	Bentonite Middle Avg. (n = 9)	Bentonite South Avg. (n = 2)	Tuff/Tuffite Avg. (n = 5)	Dacite Avg. (n = 2)	Tuff/Andesite Avg.* (n = 3)
SiO_2	45.48	50.87	47.69	66.05	70.39	65.28
Al_2O_3	12.73	16.08	20.56	14.29	15.06	10.24
Fe_2O_3	4.22	6.01	8.38	2.39	2.37	1.68
MgO	1.97	3.70	2.79	1.32	0.85	2.56
CaO	13.10	3.08	2.25	2.26	3.33	3.51
Na_2O	1.14	1.56	0.74	2.68	3.76	1.81
K_2O	1.32	1.63	2.81	2.60	1.28	1.27
TiO_2	0.63	0.78	0.93	0.40	0.27	0.24
P_2O_5	0.07	0.12	0.06	0.08	0.08	0.11
MnO	0.06	<0.06	0.06	0.05	0.04	0.03
Cr_2O_3	0.02	0.02	0.02	0.01	0.01	0.005
TOT/C	2.79	0.81	0.16	0.12	<0.02	1.04
TOT/S	0.03	<0.15	<0.34	<0.02	<0.02	0.04
LOI	18.77	15.87	13.5	7.72	2.5	13.1
Total	99.85	99.79	99.76	99.84	99.88	99.92
CIW	38.28	68.29	79.46	–	–	–
Trace elements (ppm)						
Ni	40.4	96.71	58.9	14.0	5.8	19.4
Sc	9.33	14.78	23	5	5	3.3
Ba	204.67	347.64	535	478	478.5	550.2
Be	<2	<2.78	2.5	2	<1	1.3
Co	14.67	25.20	23.75	7.4	3.5	6.2
Cs	4.0	5.98	9.05	5.6	1.0	2.0
Ga	13.53	18.06	23.1	15.0	14.1	7.33
Hf	3.57	4.31	4.85	3.8	3.7	2.8
Nb	15.53	19.16	18.65	23.7	4.3	14.9
Rb	49.43	78.20	129.9	94.6	30.5	39.7
Sn	<1	<2.22	3	<1	<1	1.3
Sr	336.37	213.96	270.9	357.0	244.8	882.6
Ta	1.14	1.48	1.25	1.9	0.4	1.3
Th	10.40	15.09	14.2	17.4	7.7	10.2
U	2.13	4.80	3.45	4.8	1.9	4.4

https://doi.org/10.1346/CCMN.2017.064051 Published online by Cambridge University Press

Table 2 (*contd*.)

Trace elements (ppm)	Bentonite North Avg. (n = 3)	Bentonite Middle Avg. (n = 9)	Bentonite South Avg. (n = 2)	Tuff/Tuffite Avg. (n = 5)	Dacite Avg. (n = 2)	Tuff/Andesite Avg.* (n = 3)
V	86.67	111.89	203	38	38	32.6
W	1.83	<1.52	1.85	1.8	1.6	0.8
Zr	136.80	154.48	176.3	138.9	139.4	83
Y	13.13	19.04	24.5	14.4	11.5	13.4
La	27.93	31.67	37.6	27.8	18.6	19.2
Ce	52.53	62.31	74.6	52.1	31.3	35.6
Pr	5.34	6.54	8.27	5.30	3.32	3.98
Nd	18.63	23.67	30.65	18.0	12.4	14
Sm	3.46	4.37	5.74	3.31	2.23	2.55
Eu	0.99	1.04	1.34	0.76	0.65	0.51
Gd	3.04	4.12	5.36	2.98	2.28	2.01
Tb	0.44	0.61	0.78	0.44	0.33	0.39
Dy	2.60	3.65	4.69	2.67	2.05	2.02
Ho	0.50	0.68	0.89	0.52	0.38	0.41
Er	1.43	2.01	2.72	1.47	1.08	1.23
Tm	0.20	0.30	0.4	0.23	0.18	0.2
Yb	1.35	1.98	2.71	1.51	1.10	1.17
Lu	0.20	0.30	0.42	0.23	0.19	0.18
Mo	<0.1	<0.47	0.85	<0.2	3.3	3.4
Cu	26.73	27.30	28.2	6.5	8.3	10.6
Pb	10.80	15.31	12.45	4.7	1	13.7
Zn	30.33	47.56	73	16.4	35	27
As	8.43	15.96	36.5	<7.0	<0.5	13.6
Cd	<0.17	<0.10	<0.1	<0.1	<0.1	0.1
Sb	<0.1	<0.14	<0.1	<0.1	<0.1	0.23
Bi	0.23	<0.32	0.2	<0.1	<0.1	0.03
Ag	<0.1	<0.10	<0.1	<0.1	<0.1	<0.1
Au (ppb)	<0.5	<0.63	0.8	<0.5	<0.5	0.96
Hg	<0.05	<0.05	<0.01	<0.04	<0.01	0.06
Tl	<0.1	<0.21	<0.1	<0.1	<0.1	0.26
Se	<0.67	<0.50	<0.5	<0.5	<0.5	<0.5
Zr/TiO_2	0.02	0.02	0.02	0.04	0.05	0.03
ΣREE	131.78	164.14	200.5	131.69	87.46	97.05
$\Sigma LREE$	104.44	124.19	151.1	103.16	65.52	72.92
$\Sigma MREE$	11.04	14.48	18.79	10.68	7.91	7.91
$\Sigma HREE$	3.18	4.59	6.24	3.43	2.53	2.78
Eu/Eu*	0.96	0.78	0.73	0.74	0.89	0.70
Ce/Ce*	0.92	0.96	0.96	0.93	0.84	0.94
$(La/Sm)_N$	5.41	4.75	4.23	5.46	5.38	4.65
$(La/Yb)_N$	16.18	12.07	9.97	13.40	12.15	11.26
$(La/Lu)_N$	15.95	12.24	9.59	13.17	10.78	8.56
$(Eu/Sm)_N$	0.77	0.65	0.62	0.60	0.77	0.50
$(Gd/Yb)_N$	1.85	1.77	1.64	1.63	1.72	1.29
$(Tb/Yb)_N$	1.48	1.42	1.32	1.33	1.37	1.53
$(Tb/Lu)_N$	1.49	1.43	1.26	1.31	1.22	1.6

n: number of samples.
*: average chemical composition of tuff/andesite samples (Aker, 2013).
ΣREE = the sum of (La−Lu)+Y; $\Sigma LREE$ = the sum of La−Nd; $\Sigma MREE$ = the sum of (Sm−Ho); $\Sigma HREE$ = the sum of (Er−Lu); $Eu/Eu^* = Eu_N/\sqrt{(Sm_N * Gd_N)}$ and $Ce/Ce^* = 3Ce_N/(2La_N + Nd_N)$ (Mongelli, 1997). Where N refers to a chondrite-normalized value (Sun and McDonough, 1989) (an extended version of Table 2 is Table S1 in the Supplemental Materials section (deposited with the Editor in Chief and available at https://www.clays.org/JOURNAL/JournalDeposits.html).

https://doi.org/10.1346/CCMN.2017.064051 Published online by Cambridge University Press

Supplemental Materials section (deposited with the Editor in Chief and available at https://www.clays.org/JOURNAL/JournalDeposits.html). The average concentrations of Ni and Co in the bentonites ranged between 40.4–96.71 ppm and 14.67–25.20 ppm, respectively. The average Cr_2O_3 contents for the bentonite and volcanic host rock samples were 0.02 wt.% and ~0.01 wt.%, respectively (Table 2 and extended version of Table 2, Table S1 in the Supplemental Materials section). The average Ni values in the middle bentonite deposit (Karayatak, Ödek, Küçükhacıbey, Hancılı, Hisarcık) were as high as 96.71 ppm.

In most instances, the average metal oxide content of the volcanic host rocks was higher than the average content in the bentonites (Table 2 and extended version of Table 2, Table S1 in the Supplemental Materials section). The average Al_2O_3 content for the volcanic host rock samples ranged from 10.24 to 15.06 wt.%. The average Fe_2O_3 content ranged from 1.68 to 2.39 wt.%. The average MgO content ranged from 0.85 to 2.56 wt.%. The average K_2O content ranged from 1.27 to 2.60 wt.%. The average SiO_2 content ranged from 65.28 to 70.39 wt.%. Lastly, the average LOI value ranged from 2.50 to 13.1 wt.% (Table 2 and extended version of Table 2, Table S1 in Supplemental Materials section) and the LOI values of the volcanic host rocks were lower than the bentonites.

The mass gains and losses were based on the plots of the geochemical analyses on the isocon diagrams (Grant, 1986, 2005). These isocon plots showed that SiO_2, Na_2O, Ba, Sr, and U were depleted, while Al_2O_3, Fe_2O_3, CaO, K_2O, TiO_2, Cr, Hf, Nb, Th, V, Zr, Y, and Zn were enriched during weathering based on the best-fit isocon slope (m = 1.07) (Table 3; Figures 10a–10f). The MgO and Rb indicated the immobile character of these elements according to the best-fit isocon slope and the constant mass (m = 1). The average Zr/TiO_2 ratios in the fresh volcanic host rock samples ranged between ~0.03 and ~0.05 and suggest a dacitic to andesitic character (Table 2 and extended version of Table 2, Table S1 in Supplemental Materials section).

General elemental correlations were examined for the bentonite and volcanic samples. The Al_2O_3, Fe_2O_3, MgO, TiO_2, and Dy/Yb were negatively correlated with SiO_2, whereas Na_2O, K_2O, Sr, Nb, and Zr/Sm were positively correlated (Figures 11a–11j). The Rb+Ba to Na_2O+K_2O ratio, the Sr to Rb ratio, the Rb/Sr to Zr ratio, the Zr/Co to Zr/Ni ratio, and Ni+Co+Cr were positively correlated with $Fe_2O_3+MgO+TiO_2$ (Figures 11k–11o). The CaO was positively correlated with LOI

Table 3. Mass gains and losses of major oxides (wt.%) and trace elements (ppm) for the bentonite samples based on the isocon analysis diagram (Grant, 1986, 2005).

			Overall volume change (%)	–2.77
			Overall mass change (%)	–6.36
			Slope	1.07
Major oxides (wt.%)	Unaltered (Avg.) C^O	Altered (Avg.) C^A	Gain/Loss relative to C_i^O $\Delta C_i/C_i^O$	Gain/Loss in wt.% ΔC_i
SiO_2	65.28	48.01	–0.31	–20.32
Al_2O_3	10.24	16.46	0.51	5.17
Fe_2O_3	1.69	6.20	2.44	4.12
MgO	2.57	2.82	0.03	0.07
CaO	3.51	6.14	0.64	2.24
Na_2O	1.81	1.15	–0.41	–0.73
K_2O	1.27	1.92	0.42	0.53
TiO_2	0.24	0.78	2.04	0.49
MnO	0.03	0.06	0.87	0.03
Trace elements (ppm)				Gain/Loss in ppm
Cr	36.49	136.84	2.51	91.65
Ba	550.20	362.44	-0.38	–210.80
Hf	2.87	4.24	0.38	1.10
Nb	14.97	17.78	0.11	1.68
Rb	39.80	42.50	0.00	0.00
Sr	882.67	273.74	–0.71	–626.33
Th	10.20	13.23	0.21	2.19
U	4.43	3.46	–0.27	–1.19
V	32.67	133.85	2.84	92.67
Zr	83.07	155.86	0.76	62.88
Y	13.43	18.89	0.32	4.26
Zn	27.00	50.30	0.74	20.10

https://doi.org/10.1346/CCMN.2017.064051 Published online by Cambridge University Press

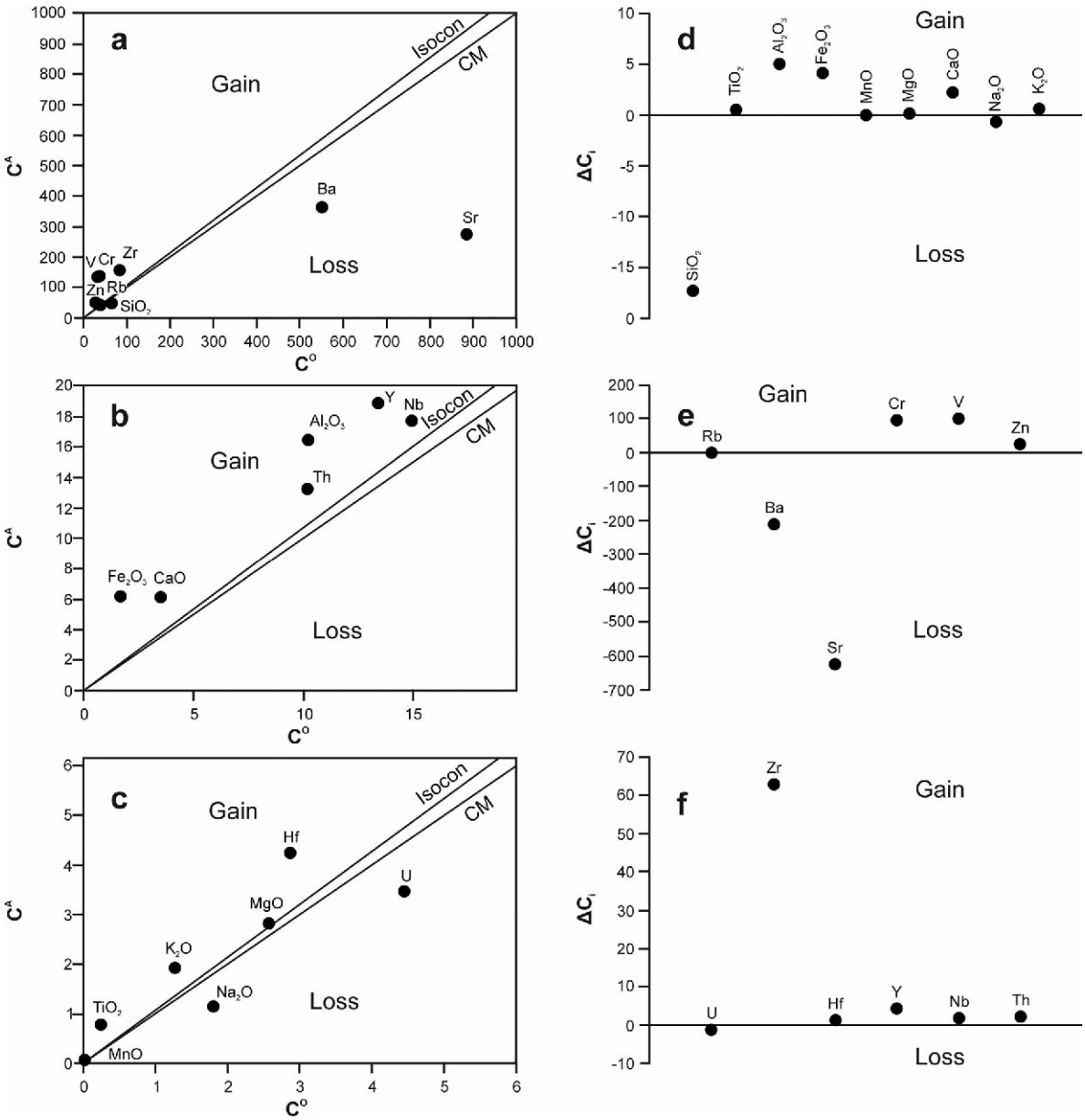

Figure 10. Mass changes (a–f) in the major element (in grams) and trace element (in ppm) contents within the study area based on the isocon analysis diagram (Grant, 1986, 2005; López-Moro, 2012). The CM line indicates a constant mass with no gain or loss.

and TOT/C (Figures 11p, 11q). The whole-rock REE contents of bentonite deposits and the related volcanic unit samples were normalized to chondrites and to the primitive mantle (Sun and McDonough, 1989; Figure 12). The *LREE* values showed an enrichment relative to *MREE+HREE* and distinct negative anomalies were observed for Eu, Ba, Nb, and Sr (Figure 12).

The calculated chemical index of weathering (CIW) values for the bentonites ranged from 18.31 to 85.10 and corresponded to a smectite concentration that ranged from 22 to 85%, a smectite+illite concentration that ranged from 36 to 96%, and a sample weathering maturity that ranged from partially weathered to completely weathered (Table 1 and Table 2; extended version of Table S1 in Supplemental Materials section). The low CIW values for MDN-5 (31.11), ODK-1 (30.47), and KBR-6 (18.31) indicated bentonites that contained significant amounts of calcite and dolomite.

Mineral chemistry

The structural formulas of smectites were calculated from the chemical analyses of the purified bentonite

https://doi.org/10.1346/CCMN.2017.064051 Published online by Cambridge University Press

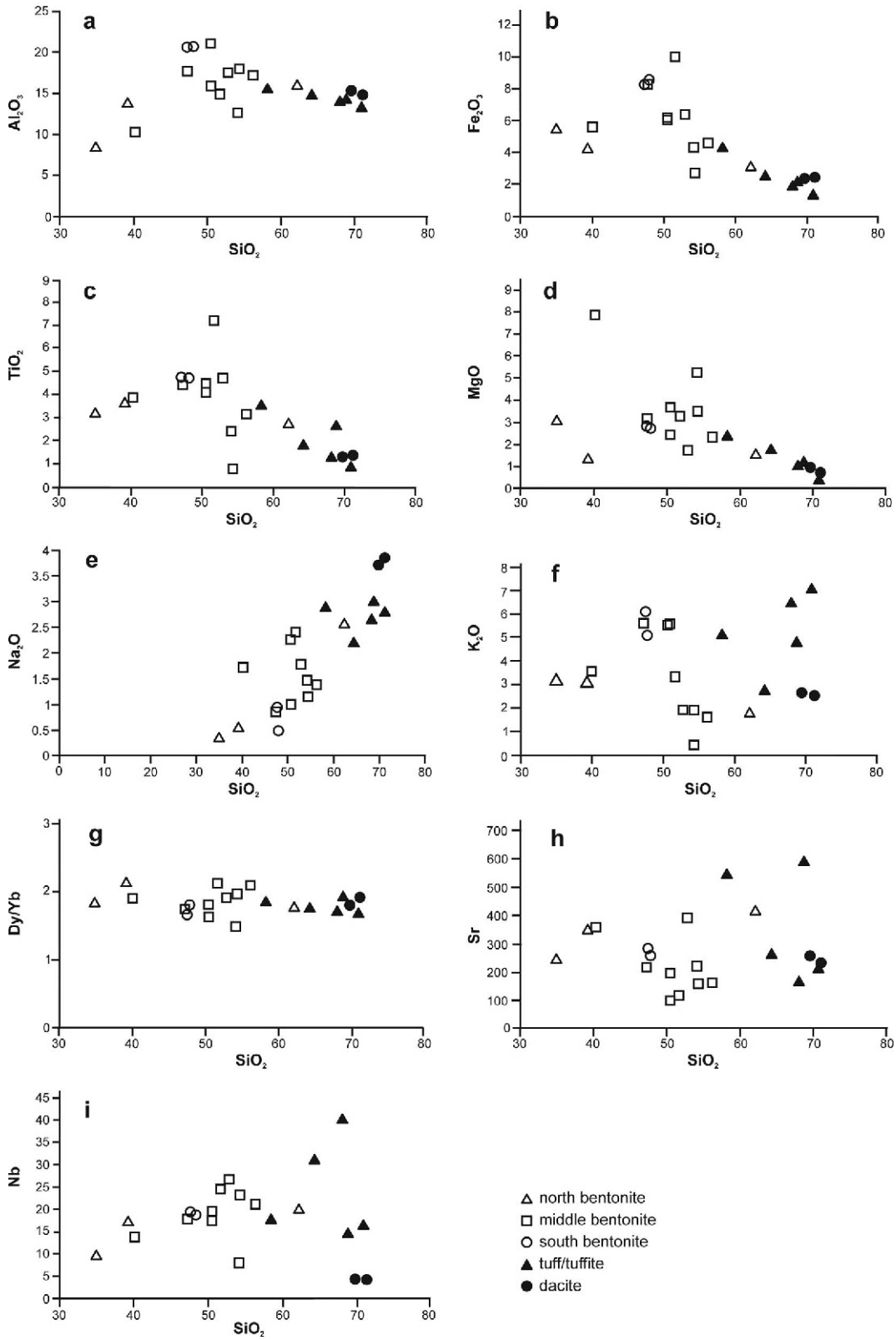

Figure 11. Elemental variation diagrams for major oxides (wt.%) and trace elements (ppm) of the bentonite and volcanic samples. (a) Al_2O_3 *vs*. SiO_2; (b) Fe_2O_3 *vs*. SiO_2; (c) TiO_2 *vs*. SiO_2; (d) MgO *vs*. SiO_2; (e) Na_2O *vs*. SiO_2; (f) K_2O *vs*. SiO_2; (g) Dy/Yb *vs*. SiO_2; (h) Sr *vs*. SiO_2; (i) Nb *vs*. SiO_2.

https://doi.org/10.1346/CCMN.2017.064051 Published online by Cambridge University Press

<2 μm samples (Table 4). The average smectite structural formula for the bentonites was $(Na_{0.33}Ca_{0.31}K_{0.18})(Al_{2.35}Fe_{0.80}Mg_{0.78})(Si_{7.79}Al_{0.21})O_{20}(OH)_4$.

The Si in the smectite tetrahedral sites in most cases contained small amounts of substituted Al and moderate amounts of Al substitution were noted for the KHB-10 bentonite. Otherwise, the layer charge for the smectites in most of these bentonites was located in the octahedral sheet. The octahedral sheet of the smectites predominantly contained Al and Fe(III) with smaller amounts of Mg. The smectite interlayer cations were dominantly Ca, Na, and K. The calculated layer charge indicated a

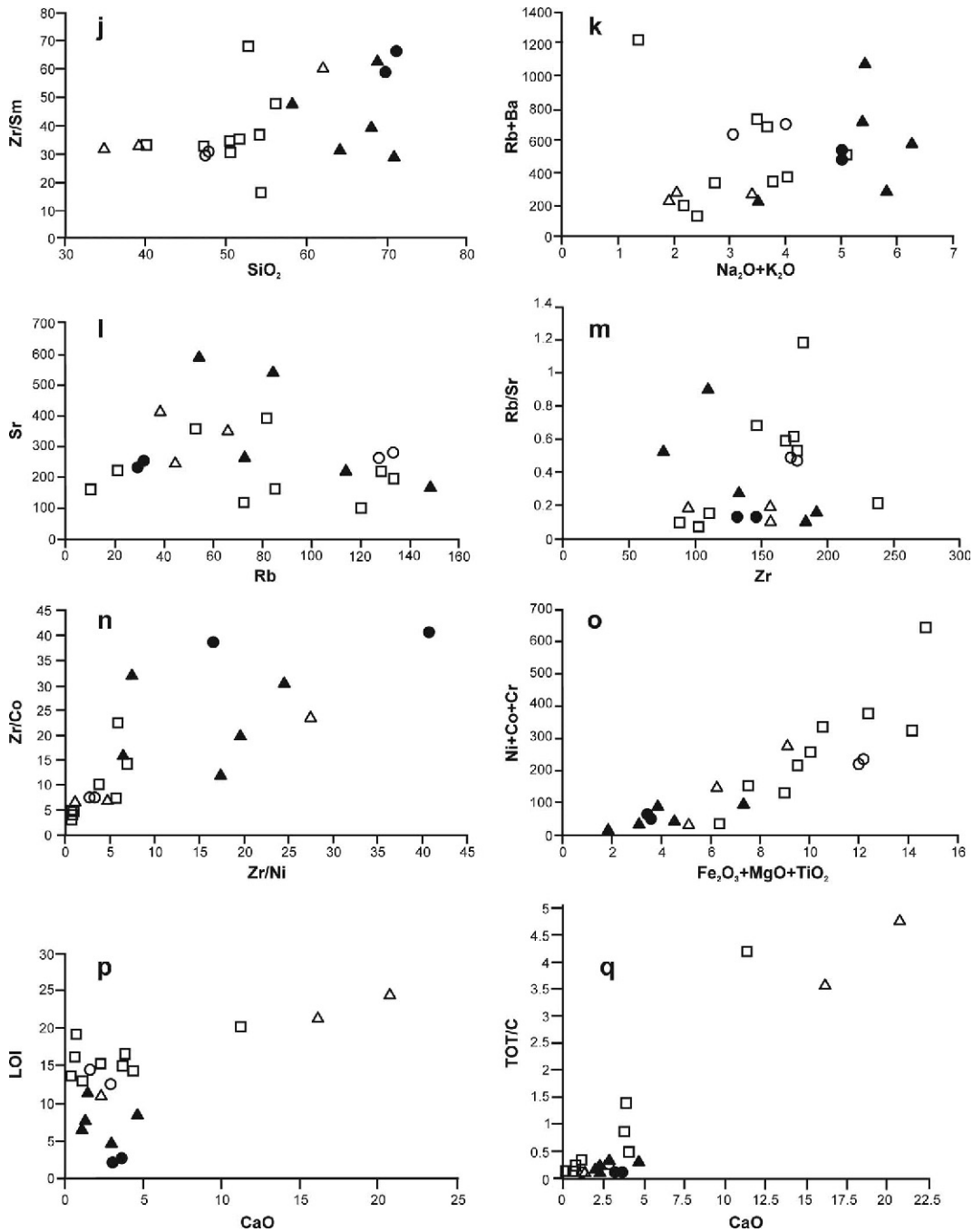

Figure 11 (*contd*.). Elemental variation diagrams for major oxides (wt.%) and trace elements (ppm) of the bentonite and volcanic samples. (j) Zr/Sm *vs*. SiO_2; (k) Rb+Ba *vs*. Na_2O+K_2O; (l) Sr *vs*. Rb; (m) Rb/Sr *vs*. Zr; (n) Zr/Co *vs*. Zr/Ni; (o) Ni+Co+Cr *vs*. $Fe_2O_3+MgO+TiO_2$; (p) LOI *vs*. CaO; (q) TOT/C *vs*. CaO.

https://doi.org/10.1346/CCMN.2017.064051 Published online by Cambridge University Press

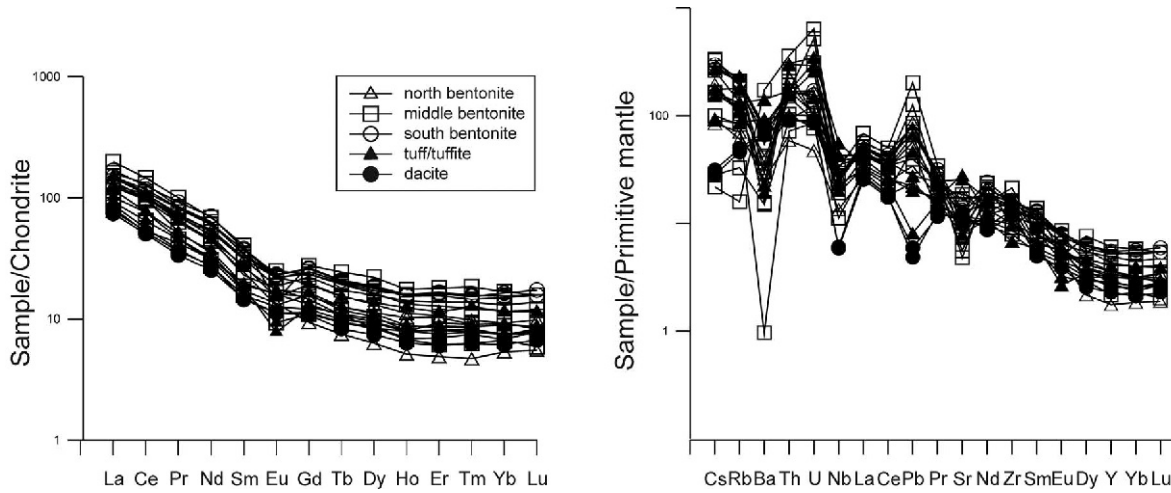

Figure 12. Chondrite and primitive mantle-normalized patterns for bentonite and volcanic samples from the Ankara-Çankırı regions (Sun and McDonough, 1989).

smectite (Z <1.2) based on a formula with the −44 layer charge contributed by the 20 oxygens and 4 hydroxyls. The $Na^+/(Na^+ + Ca^{2+})$ ratios of the smectites were 0.06, 0.8, and 0.4−0.7 based on the Takagi *et al.* (2005) classification and the ratios indicate variable interlayer compositions that ranged from Na-rich to Ca-rich.

Table 4. Chemical compositions (wt.%) and structural formulas of smectites in the bentonite samples.

Major oxides (wt.%)	KBR-3 Ca bentonite	KHB-10 Na bentonite	HNC-7 Na-Ca bentonite	HSC-8 Na-Ca bentonite	KRY-7 Na-Ca bentonite	Avg.
SiO_2	53.41	51.67	59.35	54.16	55.72	54.86
Al_2O_3	12.82	15.00	20.00	12.61	16.56	15.40
Fe_2O_3	11.38	10.02	3.21	4.30	8.12	7.41
MgO	3.26	3.28	4.06	5.27	2.54	3.68
CaO	2.93	1.11	0.76	3.86	1.27	1.99
Na_2O	0.11	2.39	1.01	1.47	0.98	1.19
K_2O	1.13	1.65	0.11	0.95	0.89	0.95
CIW	80.83	81.08	91.87	70.29	88.04	82.42
SiO_2/Al_2O_3	4.17	3.44	2.97	4.30	3.36	3.65
Tetrahedral						
Si	7.77	7.55	7.88	7.97	7.83	7.79
Al	0.23	0.45	0.12	0.03	0.17	0.21
Σ	8.00	8.00	8.00	8.00	8.00	8.00
Octahedral						
Al	1.97	2.13	3.02	2.16	2.57	2.35
Fe	1.25	1.10	0.32	0.48	0.86	0.80
Mg	0.71	0.71	0.80	1.16	0.53	0.78
Σ	3.93	3.95	4.14	3.80	3.96	3.96
Interlayer						
Ca	0.46	0.17	0.11	0.61	0.19	0.31
Na	0.03	0.68	0.26	0.42	0.27	0.33
K	0.21	0.31	0.02	0.18	0.16	0.18
Σ	0.70	1.16	0.39	1.21	0.62	0.82
$Na^+/(Na^+ + Ca^{2+})$	0.06	0.8	0.7	0.4	0.58	0.51
Tetrahedral charge	0.23	0.45	0.12	0.03	0.17	0.21
Octahedral charge	0.92	0.88	0.38	1.79	0.64	0.91
Total charge	1.15	1.33	0.50	1.82	0.81	1.12
Interlayer charge	1.15	1.33	0.50	1.82	0.81	1.12

https://doi.org/10.1346/CCMN.2017.064051 Published online by Cambridge University Press

DISCUSSION

The newly studied and economically valuable bentonite deposits occur within the Miocene lacustrine volcanic/sedimentary rocks of the Ankara-Çankırı basin of central Anatolia (Figure 13). The volcanic and sedimentary rocks consist of limestone and the clastic rocks consist of conglomerate, sandstone, siltstone, tuff/tuffite, andesite, and dacite. The host rocks of the bentonite deposits are mainly and in most instances the tuff/tuffite, dacite, and andesite of the Hancılı Formation. The alternation of yellow, green, and brown bentonites and argillaceous tuffaceous sediments reflect the fluctuations between reducing and oxidizing conditions in the environment during the deposition of the tuffaceous sediments (Li *et al*., 2016). Desiccation cracks, locally enclosed coal seams, plant rootlets, gypsum lenses, yellow sulfate-like fracture infillings, and iron oxide stains also indicate a shallow lacustrine environment (Wright and Tucker, 1991).

Bentonite deposits in the study area have primary features that suggest bentonites, such as abundant smectite and clay-rich rocks that are locally interbedded within carbonate rocks. The abundance of smectite, the absence of sorting, and detrital materials in the basin suggest that primary bentonites were formed after the deposition of ash flow tuff or air flow tuff rather than secondary bentonites (Jeans *et al*., 1982). The position of the bentonite layers and the interbedded carbonates suggest that these ash materials were deposited in a calm lacustrine environment. After deposition, the ash materials were subjected to early diagenetic weathering processes, such as feldspar+amphibole+biotite+glass to clay reactions.

The bentonites also exhibit local secondary diagenetic characteristics based on an increased chlorite content southward of the basin and high concentrations of Al_2O_3, Fe_2O_3, and K_2O in strata beneath and above the bentonites. The presence of subrounded volcanic and ophiolitic fragments in a volcanic groundmass of tuffitic host rocks suggests that volcanic and terrigenous materials were transported into a lacustrine depositional environment in the study area and formed the local occurrences of secondary bentonites (Jeans *et al.*,1982). Furthermore, the local presence of rounded to subrounded ophiolitic clasts and terrigenous materials in bentonites may suggest that these bentonites were formed following the re-deposition of pyroclastic and ophiolitic materials in the Karahöyük bentonite deposit and in the lower levels of the Saray, Hisarcık, and Hancılı bentonite deposits (samples SRY-1, HSC-1, HSC-4, HNC-3; Figure 4) close to the ophiolitic basement units.

Texturally and micromorphologically, smectite flakes were found covering phenocrysts as well as within the matrix between degraded feldspar, volcanic glass, and oxidized biotite and hornblende. The formation of smectite was likely driven by the dissolution of volcanic phenocrysts by chemical weathering processes during early diagenesis (Christidis and Dunham; 1997; Deschamps *et al*., 2012; Külah *et al.*, 2014; Ekinci Şans *et al*., 2015; Kadir *et al*., 2015).

The leaching of SiO_2, Na_2O, Ba, Sr, and U, and the enrichment of Al_2O_3, Fe_2O_3, CaO, K_2O, TiO_2, Cr, Hf,

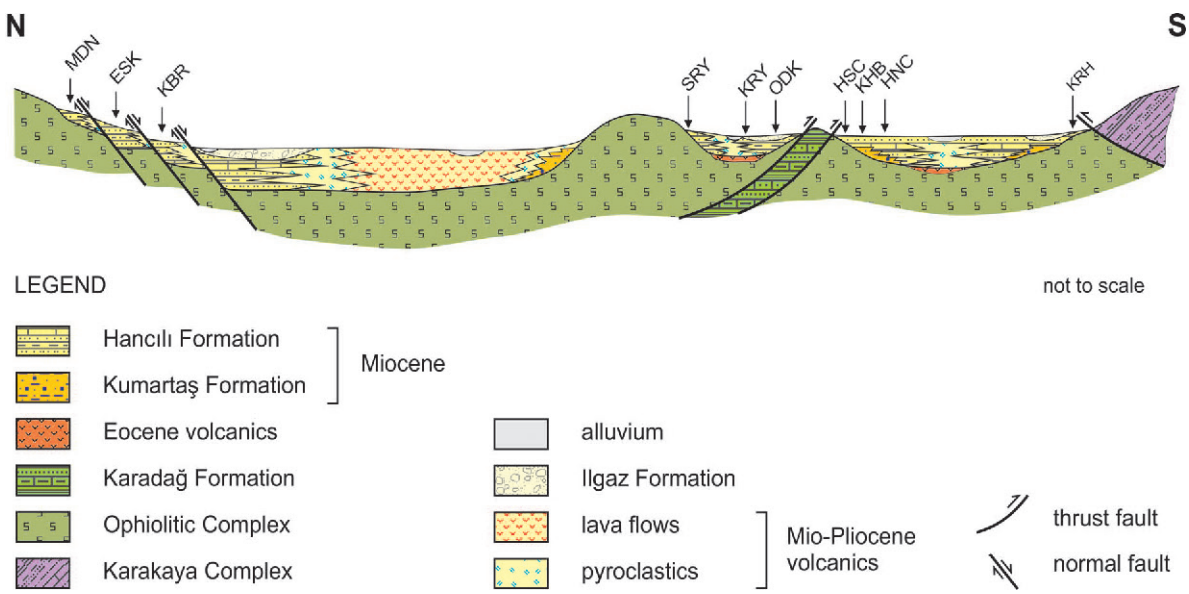

Figure 13. Genetic model for the Ankara-Çankırı bentonite deposits.

https://doi.org/10.1346/CCMN.2017.064051 Published online by Cambridge University Press

Nb, Th, V, Zr, Y, and Zn during the alteration of plagioclase, K-feldspar, biotite, hornblende, and volcanic glass that were derived from volcanic units favored the precipitation of smectite under alkaline conditions (Nesbitt and Young, 1984; Christidis, 1998; Yan *et al.*, 2016, Figures 10a–10f). The enrichment of Zr and Hf was possibly related to the fractionation of zircon and biotite (Tsikouras *et al.*, 2016). The immobility of the MgO and Rb developed during the alteration of volcanogenic materials in alkaline lakes (Summa and Verosub, 1992; Özdamar *et al.*, 2014) (Table 3; Figures 10a–10f).

The following correlations were noted to further support that the source of smectite was the weathering of volcanic materials. (1) The negative correlation between Al_2O_3 and SiO_2 and the positive correlations between Na_2O and K_2O with SiO_2 were related to the fractional crystallization of plagioclase, K-feldspar, and volcanic glass (Wulaningsih *et al.*, 2013; Figure 11). (2) The increased Sr and decreased Rb and Ba contents relative to SiO_2 and the positive correlation between Rb+Ba and Na_2O+K_2O may indicate fractionation of Na- and K-feldspar and the concentration of Na and K in the clay fractions (Motoki *et al.*, 2015). (3) The positive correlations between Sr and Rb, between Rb/Sr and Zr, and between Zr/Co and Zr/Ni also suggest fractionation of plagioclase (Ghanem and Jarrar, 2013). The negative correlations between Fe_2O_3, TiO_2, and Dy/Yb with SiO_2 and the positive correlation between Zr/Sm and SiO_2 may indicate fractionation of amphibole (Aydınçakır and Şen, 2013; Wang *et al.*, 2015).

The relative increases in the *LREE/(MREE+HREE)* ratios, the similarity of the REE plots for the bentonite and volcanic host rock samples, and the negative Eu anomaly suggest that smectite precipitation was most likely caused by the chemical weathering of feldspar, hornblende, and devitrified volcanic glass that were derived from volcanic units under oxidizing and reducing sedimentation environments (Zielinski, 1982; Christidis, 1998; Kadir *et al.*, 2002, 2014; Zhou *et al.*, 2013; Külah *et al.*, 2014).

The enrichment of Fe_2O_3, Cr, Ni, and Cu suggests a contribution of the ophiolitic source rock (Butt and Cluzel, 2013; Külah *et al.*, 2014; Kadir *et al.*, 2015). This interpretation was also supported by the increased Fe_2O_3 contents in the bulk bentonite samples and indicated the abundance of smectite associated with chlorite in the middle and southern areas of the study. The Cr, Ni, V, and Nb (and related Fe_2O_3) contents may indicate that these trace elements either occur in the structures of the Fe-(oxyhydr)oxide phases, are adsorbed to smectites, or occupy octahedral sites in smectites (Abedini and Calagari, 2012; Becquer *et al.*, 2006; Dublet *et al.*, 2015). The low values and the positive correlation between Ni+Co+Cr and $Fe_2O_3+MgO+TiO_2$ may suggest a local contribution of these immobile elements from the ophiolitic basement rock units. The relative decrease of MgO with an increase in SiO_2 may indicate fractionation of olivine and pyroxene that originated from ophiolitic materials (Assah *et al.*, 2015; Wang *et al.*, 2015; Torres-Alverado *et al.*, 2016; Lai *et al.*, 2017). These results are consistent with the conclusions reported by Venturelli *et al*. (1997), Freyssinet *et al*. (2005), Fan and Gerson (2011), and Kadir *et al*. (2013, 2015).

Additionally, a positive correlation between CaO with the LOI and TOT/C values suggests that calcite and dolomite were precipitated as chemical sediments in the lake and were later subjected to diagenesis (Figures 11p, 11q). The $Na^+/(Na^+{+}Ca^{2+})$ ratios of the bentonites suggest that the smectites have variable interlayer compositions that ranged from Ca-rich interlayers to Na-rich interlayers. The ratios in some instances showed roughly equal amounts of Ca and Na. The $Na^+/(Na^+{+}Ca^{2+})$ ratios were also supported by the XRD peaks of oriented smectite samples. The d_{001} peaks at 14.12–14.87 Å and 12.67 Å are indicative of Ca-smectite and Na-smectite, respectively. The average major element composition yielded a structural formula that corresponds to a montmorillonitic smectite:

$$(Na_{0.33}Ca_{0.31}K_{0.18})(Al_{2.35}Fe_{0.80}Mg_{0.78})(Si_{7.79}Al_{0.21})O_{20}(OH)_4.$$

The field observations and the mineralogical and geochemical determinations suggest that the bentonites were formed mainly under chemical weathering of volcanogenic materials during early diagenesis. Furthermore, the compaction of the bentonite units, the oxidation of Fe in hornblende and biotite, and the precipitation of euhedral micritic dolomite in the pores of a flaky smectite also support precipitation under diagenetic conditions (Zaid and Gahtani, 2015).

CONCLUSIONS

The Ankara-Çankırı bentonite deposits in central Anatolia formed from Miocene volcanic/sedimentary units that consisted of bentonite, andesitic tuff/tuffite units, and local interbeds of organic materials. These lithologic provenance relationships suggest that the primary and locally secondary bentonites were formed under alkaline, shallow, and swampy lacustrine depositional conditions controlled by periodic climatic changes. The gradational contact between the bentonite and an intercalated argillized tuff and the smectite flake edges with degraded feldspar and devitrified volcanic glass suggest dissolution from a weathered feldspar surface, and that smectite precipitation was the primary mode for smectite formation rather than the weathering of volcanic glass which supports the second hypothesis. Degradation of K-feldspar, plagioclase, and the oxidation of Fe in hornblende and biotite resulted in increased concentrations of Al_2O_3, Fe_2O_3, and MgO, which were available for the precipitation of smectite under the

https://doi.org/10.1346/CCMN.2017.064051 Published online by Cambridge University Press

alkaline physicochemical environmental conditions that were controlled by a closed hydrologic system. The bentonite interlayer cation compositions were Ca, Na, and Na-Ca based on the interlayer cation ratios and the smectite XRD basal reflection values. The high *LREE*/(*MREE*+*HREE*) ratios and similarity of these ratios, the negative Eu anomalies, the positive correlation between the Zr/Ni ratios and the Zr/Co ratios, and the positive correlation between Rb+Ba and Na_2O+K_2O suggest that smectite formed from volcanic materials during chemical weathering processes. On the basis of the restricted slight increases in chlorite content, the Cr+Ni values, the $Fe_2O_3+MgO+TiO_2$ values, and the negative correlation between MgO and SiO_2 indicate that ophiolitic materials from the basement units contributed to the formation of the bentonites in the basin.

ACKNOWLEDGMENTS

This present study was supported financially by the Scientific Research Projects Fund of Eskişehir Osmangazi University in the framework of Project 2014–656. Professor Daniel M. Deocampo is greatly thanked for calculating the semi-quantitative estimates of mineral abundance. The X-ray diffractometer used at Georgia State University, USA, was purchased with funds from the National Science Foundation, Award # 1029020 to Professors Daniel M. Deocampo and W. Crawford Elliott. The authors are also extremely grateful to Professor J. Marion Wampler (Georgia State University, USA) for detailed reviews and suggestions on an early draft of the manuscript. The authors are much indebted to an anonymous reviewer and to an anonymous Associate Editor for their extremely careful and constructive reviews that improved the quality of the paper significantly. This paper was presented at the 53rd Annual Meeting of The Clay Minerals Society, Atlanta, Georgia, USA, 2016.

REFERENCES

Abedini, A. and Calagari, A.A. (2012) The mineralogy and geochemistry of Permian lateritic ores in east of Shahindezh, West-Azarbaidjan province. *Iranian Journal of Crystallography and Mineralogy*, **20**, 59–72.

Aker, S. (2013) *Evaluation of a Cenozoic Lacustrine Basin – Hancılı Formation (Kalecik-Ankara) and its Paleoenvironment and Paleoclimate Analysis Based on Mineral Facies*. PhD Thesis. Middle East Technical University, 94 pp.

Akyürek, B., Duru, M., Sütçü, Y.F., Papak, Şaroğlu, F., Pehlivan, N., Gönenç, O., Granit, S., and Yaşar, T. (1996) *Ankara ilinin çevre jeolojisi ve doğal kaynaklar projesi (1994 yılı jeoloji grubu çalı*şmaları). MTA Rapor No: 9961, Ankara, [Environmental Geology and Natural Resources Project of Ankara (1994 Geological Group Studies) MTA Report No. 9961, Ankara, Turkey].

Assah, A.N.E., Yokoyama, T., Aka, F.T., Usui, T., Wirmvem, M.J., Tchamabe, B.C., Ohba, T., Tanyileke, G., and Hell, J.V. (2015) A comparative review of petrogenetic processes beneath the Cameroon Volcanic Line: Geochemical constraints. *Geoscience Frontiers*, **6**, 557–570.

Aydınçakır, E. and Şen, C. (2013) Petrogenesis of the post-collisional volcanic rocks from the Borçka (Artvin) area: Implications for the evolution of the Eocene magmatism in the Eastern Pontides (NE Turkey). *Lithos*, **172-173**, 98–117.

Bakır, S., Akbulut, A., Kapkaç, F., Karahan, D.S., and Çetin C. (2012) *Türkiye Bentonit Envanteri* (Envanter Serisi 204*), Maden Tetkik ve Arama Genel Müdürlüğü, Ankara* [*Turkey Bentonite Inventory (Inventory Series 204), Ankara, Turkey, General Directorate of Mineral Research and Exploration*].

Becquer, T., Quantin, C., Rotte-Capet, S., Ghanbaja, J., Mustin, C., and Herbillon, A.J. (2006) Sources of trace metals in Ferralsols in New Caledonia. *European Journal of Soil Science*, **57**, 200–213.

Butt, C.R.M. and Cluzel, D. (2013) Nickel laterite ore deposits: weathered Serpentinites. *Elements*, **9**, 123–128.

Chamley, H. (1989) *Clay Sedimentology*, Springer Verlag, New York, 623 pp.

Christidis, G.E. (1998) comparative study of the mobility of major and trace elements during alteration of an andesite and a rhyolite to bentonite, in the islands of Milos and Kimolos, Aegean, Greece. *Clays and Clay Minerals*, **46**, 379–399.

Christidis, G. and Dunham, A.C. (1997) Compositional variations in smectites. Part II: Alteration of acidic precursors. A case study from Milos Island, Greece. *Clay Minerals*, **32**, 253–270.

Christidis, G.E. and Huff, W.D. (2009) Geological aspects and genesis of bentonites. *Elements*, **5**, 93–98.

Dangerfield, A., Harris, R., Sarıfakıoğlu, E., and Dilek, Y. (2011) Tectonic evolution of the Ankara Mélange and associated Eldivan ophiolite near Hançılı, central Turkey. In *Mélanges: Processes of Formation and Societal Significance* (J. Wakabyashi and Y. Dilek, editors). Geological Society of America Special Paper 480, 143–169, doi: 10.1130/2011.2480(06).

Deschamps, R., Kohler, E., Gasparrini, M., Durand, O., Euzen, T., and Nader, F. (2012) Impact of mineralogy and diagenesis on reservoir quality of the Lower Cretaceous Upper Mannville Formation (Alberta, Canada). *Oil and Gas Science and Technology-Rev. IFP Energies nouvelles*, **67**, 31–58.

Ddani, M., Meunier, A., Zahraoui, M., Beaufort, D., El Wartiti, M., Fontaine, C., Boukili, B., and El Mahi, B. (2005) Clay mineralogy and chemical composition of bentonites from the Gourougou volcanic massif, Northeast Morocco. *Clays and Clay Minerals*, **53**, 250–267.

Dilek, Y. and Thy, P. (2006) Age and petrogenesis of plagiogranite intrusions in the Ankara mélange, central Turkey. *Island Arc*, **15**, 44–57.

Dönmez, M. and Akçay, A.E. (2010) Geological Map of Çankırı H 30 Quadrangle, Scale 1:100.000, *General Directorate of Mineral Research and Exploration (MTA) Publications*, Ankara, Turkey.

Dublet, G., Juillot, F., Morin, G., Fritsch, E., Fandeur, D., and Brown Jr., G.E. (2015) Goethite aging explains Ni depletion in upper units of ultramafic lateritic ores from New Caledonia. *Geochimica et Cosmochimica Acta*, **160**, 1–15.

Ekinci Şans, B., Esenli, F., Kadir, S., and Elliott, W.C. (2015) Genesis of smectite in siliciclastics and pyroclastics of the Eocene İslambeyli Formation in the Lalapaşa region, NW Thrace, Turkey. *Clay Minerals*, **50**, 459–483.

Fan, R. and Gerson, A.R. (2011) Nickel geochemistry of a Philippine laterite examined by bulk and microprobe synchrotron analyses. *Geochimica et Cosmochimica Acta*, **75**, 6400–6415.

Freyssinet, P., Butt, C.R.M., Morris, R.C., and Piantone, P. (2005) Ore-forming processes related to lateritic weathering, in *Economic Geology 100th Anniversary Volume*, p. 681–722, Appendix (CD) 7 pp.

Ghanem, H. and Jarrar, G.H. (2013) Geochemistry and petrogenesis of the 595 Ma shoshonitic Qunai monzogabro, Jordan. *Journal of African Earth Sciences*, **88**, 1–14.

Gökten, E. and Floyd, P.A. (2007) Stratigraphy and geochemistry of pillow basalts within the ophiolitic mélange of the İzmir-Ankara-Erzincan suture zone: implications for the geotectonic character of the northern branch of Neotethys. *International Journal of Earth Sciences*, **96**, 725–741.

Göncüoğlu, M.C., Yalınız, K., and Tekin, U.K. (2006) Geochemistry, tectono-magmatic discrimination and radiolarian ages of basic extrusives within the Izmir-Ankara suture belt (NW Turkey): Time constraints for the Neotethyan evolution. *Ofioliti*, **31**, 25–38.

Grant, J.A. (1986) The isocon diagram – a simple solution to Gresens' equation for metasomatic alteration. *Economic Geology*, **81**, 1976–1982.

Grant, J.A. (2005) Isocon analysis: A brief review of the method and applications. *Physics and Chemistry of the Earth*, **30**, 997–1004.

Hakyemez, Y., Barkurt, M.Y., Bilginer, E., Pehlivan, Ş., Can, B., Dağer, Z., and Sözeri, B. (1986) *General Directorate of Mineral Research and Exploration*, Report No. 7966, 114s, Ankara, Turkey (unpublished).

Huff, W. D., Anderson, T. B., Rundle, C. C., and Odin G. S. (1991) Chemostratigraphy, K-Ar ages and illitization of Silurian K-bentonites from the Central Belt of the Southern Uplands-Down-Longford terrane, British Isles. *Journal of the Geological Society*, **148**, 861–868.

Huff, W.D. (2016) K-bentonites: A review. *American Mineralogist*, **101**, 43–70.

Jeans, C.V., Merriman, R.J., Mitchell, J.G., and Bland, D.J. (1982) Volcanic clays in the Cretaceous of southern England and northern Ireland. *Clay Minerals*, **17**, 105–156.

Kadir, S., Baş, H., and Karakaş, Z. (2002) Origin of sepiolite and loughlinite in a Neogene volcano–sedimentary lacustrine environment, Mihalıççık–Eskişehir, Turkey. *The Canadian Mineralogist*, **40**, 1091–1102.

Kadir, S., Kolaylı, H., and Eren, M. (2013) Genesis of sedimentary– and vein–type magnesite deposits at Kop Mountain, NE Turkey. *Turkish Journal of Earth Sciences*, **22**, 98–114.

Kadir, S., Eren, M., Külah, T., Önalgil, N., Cesur, M., and Gürel, A. (2014) Genesis of late Miocene–Pliocene lacustrine palygorskite and calcretes from Kırşehir, central Anatolia, Turkey. *Clay Minerals*, **49**, 473–494.

Kadir, S., Aydoğan, M.S., Elitok, Ö., and Helvacı, C. (2015) Composition and genesis of nickel-chrome-bearing nontronite and montmorillonite in lateritized ultramafic rocks in the Muratdagi region (Uşak, western Anatolia), Turkey. *Clays and Clay Minerals*, **63**, 163–184.

Karadenizli, L., Seyitoğlu, G., Saraç, G., Kazancı, N., Şen, Ş., Hakyemez, Y., and Savaşçı, D. (2003) Çankırı-Çorum havzası batı kenarının erken-orta Miyosen paleocoğrafik evrimi. *Maden Tetkik ve Arama Dergisi (Mining Investigation and Search Magazine)*, **126**, 69–86.

Kaymakçı, N. (2000) *Tectono-stratigraphical Evolution of the Çankırı Basin* (Central Anatolia, Turkey). PhD Thesis. University Utrecht Geological Ultraiectina, no: 190, 247 pp.

Koçyiğit, A., Türkmenoğlu, A., Beyhan, Kaymakçı, N., and Akyol, E. (1995) Post-Collisional tectonics of Eskişehir-Ankara-Çankırı segment of İzmir-Ankara-Erzincan suture zone: Ankara Orogenic Phase. *Türkiye Petrol Jeologları Derneği Bülteni (Turkish Petroleum Geologists Association Bulletin)*, **6**, 69–86.

Külah, T., Kadir, S., Gürel, A., Eren, M., and Önalgil, N. (2014) Mineralogy, geochemistry, and genesis of mudstones in the upper Miocene Mustafapaşa member of the Ürgüp formation in the Cappadocia region, central Anatolia, Turkey. *Clays and Clay Minerals*, **62**, 267–285.

Kunze, G.W. and Dixon, J.B. (1986) Pretreatment for mineralogical analysis. Pp. 91–100 in: *Methods of Soil Analysis, Part 1. Physical and Mineralogical Methods* (2nd edition) (A. Klute, editor). American Society of Agronomy, Inc. and the Soil Science Society of America, Inc., Madison, Wisconsin, USA.

Lai, Y.-M., Song, S.-R., Lo, C.-H., Lin, T.-H., Chu, M.-F., and Chung, S.-L. (2017) Age geochemical and isotopic variations in volcanic rocks from the Coastal Range of Taiwan: Implications for magma generation in the Northern Luzon Arc. *Lithos*, **272-273**, 92–115.

Li, Y., Cai, J., Song, M., Ji, J., and Bao, Y. (2016) Influence of organic matter on smectite illitization: A comparison between red and dark mudstones from the Dongying Depression, China. *American Mineralogist*, **101**, 134–145.

López-Moro, F.J. (2012) EASYGRESGRANT – A Microsoft Excel spreadsheet to quantify volume changes and to perform mass-balance modeling in metasomatic systems. *Computers and Geosciences*, **39**, 191–196.

Moe, J.A., Ryan, P.C., Elliott, W.C., and Reynolds, R.C. (1996) Petrology, chemistry, and clay mineralogy of a K-bentonite in the Proterozoic Belt Supergroup of Western Montana. *Journal of Sedimentary Research*, Part A., **66**, 95–99.

Moore, D.M. and Reynolds, R.C. (1989) *X-ray Diffraction and the Identification and Analysis of Clay Minerals*. Oxford University Press, New York, 332 pp.

Mongelli, G. (1997) Ce-anomalies in the textural components of Upper Cretaceous karst bauxites from the Apulian carbonate platform (southern Italy). *Chemical Geology*, **140**, 69–79.

Motoki, A., Sichel, S.E., Vargas, T., Melo, D.P., and Motoki, K.F. (2015) Geochemical behaviour of trace elements during fractional crystallization and crustal assimilation of the felsic alkaline magmas of the state of Rio de Janeiro, Brazil. *Anais da Academia Brasileira de Ciências (Annals of the Brazilian Academy of Sciences)*, **87**, 1959–1979.

Nesbitt, H.W. and Young, G.M. (1984) Prediction of some weathering trends of plutonic and volcanic rocks based on thermodynamic and kinetic considerations. *Geochimica et Cosmochimica Acta*, **48**, 1523–1534.

Newman, A.C.D. and Brown, G. (1987) The interaction of water with clay mineral surfaces. Pp. 1–128 in: *Chemistry of Clays and Clay Minerals* (A.C.D. Newman, editor). Wiley, New York, USA.

Okay, A.İ. and Tüysüz, O. (1999) Tethyan Sutures of Northern Turkey. *Geological Society, London, Special Publications*, **156**, 475–515.

Osborn, S.G., Duffield, L.T., Elliott, W.C., Wampler, J.M., Elmore, R.D., and Engel, M.H. (2014) The timing of diagenesis and thermal maturation of the Cretaceous Marias River Shale, Disturbed Belt, Montana. *Clays and Clay Minerals*, **62**, 112-125.

Özdamar, Ş., Ece, Ö.I., Uz, B., Boylu, F., Ercan, H.Ü., and Yanık, G. (2014) Element mobility during the formation of the Uzunisa-Ordu bentonite, NE Turkey, and potential applications. *Clay Minerals*, **49**, 609-633.

Paz, S.P.A., Angélica, R.S., and Neves R.F. (2012) Mg-bentonite in the Parnaíba Paleozoic Basin, Northern Brazil. *Clays and Clay Minerals*, **60**, 265–277.

Ray, D.C., Collings, A.J.V., Worton, G.J., and Jones, G. (2011) Upper Wenlock bentonites from Wren's Nest Hill, Dudley: comparisons with prominent bentonites along Wenlock Edge, Shropshire, England. *Geological Magazine, Cambridge University Press*, **148**, 670–681.

Rojay, B. (2013) Tectonic evolution of the Cretaceous Ankara Ophiolitic Mélange during the Late Cretaceous to pre-Miocene interval in Central Anatolia, Turkey. *Journal of Geodynamics*, **65**, 66–81.

Ross, C.S. and Shannon, E.V. (1926) The minerals of bentonite and related clays and their physical properties. *American Ceramic Society Journal*, **9**, 77–96.

Sevin, M. and Uğuz, M.F. (2011) Geological Map of Çankırı G 30 Quadrangle, Scale 1:100.000, *General Directorate of Mineral Research and Exploration (MTA) Publications*, Ankara, Turkey.

Seyitoğlu, G., Kazancı, N., Karadenizli, L., Şen, Ş., Varol, B., and Karabıyıkoğlu, T. (2000) Rockfall avalanche deposits associated with normal faulting in the NW of Çankırı basin: Implications for the post-collisional tectonic evolution of the Neo-Tethyan suture zone. *Terra Nova*, **12**, 245–251.

Środoń, J., Clauer N., Banas, M., and Wójtowicz, A. (2006) K-Ar evidence for a Mesozoic thermal event superimposed on burial diagenesis of the Upper Silesia Coal Basin. *Clay Minerals*, **41**, 669–690.

Summa, L.L. and Verosub, K.L. (1992) Trace element mobility during early diagenesis of volcanic ash: applications to stratigraphic correlation. *Quaternary International*, **13-14**, 149–157.

Sun, S.-S. and McDonough, W.F. (1989) Chemical and isotopic systematics of oceanic basalts: implications for mantle composition and processes. *Geological Society Special Publications*, **42**, 313–345.

Takagi, T., Koh, S.M., Song, M.S., Itoh, M., and Mogi, K. (2005) Geology and properties of the Kawasaki and Dobuyama bentonite deposits of Zao region in northeastern Japan. *Clay Minerals*, **40**, 333–350.

Torres-Alverado, I.S., Lenhardt, N., Arce, J.L., and Hinderer, M. (2016) Geochemical and isotopic composition of volcanic rocks of the heterogeneous Miocene (~23–19 Ma) Tepoztlán Formation, early Transmexican Volcanic Belt, Mexico. *Journal of Volcanology and Geothermal Research*, **316**, 72–84.

Tsikouras, B., Passa, K.-S., Iliopoulos, I., and Katagas, C. (2016) Microstructural control on perlite expansibility and geochemical balance with a novel application of isocon analysis: An example from Milos Island perlite (Greece). *Minerals*, **6**, 1–14.

Türkmenoğlu, A.G., Akıman, O., Aker, S., and Tankut, A. (1991) Geology and origin of clay deposits at Orta (Çankırı) area. *Bulletin of the Mineral Research and Exploration*, **113**, 87–92.

Tüysüz, O. and Dellaloğlu, A.A. (1992) Çankırı havzasının tektonik birlikleri ve jeolojik evrimi. Türkiye 9. *Petrol Kongresi Bildirileri (Petroleum Congress Reports)*, 1–17.

Vitali, F., Blanc, G., Larqué, P., Duplay, J., and Morvan, G. (1999) Thermal diagenesis of clay minerals within volcanogenic material from the Tonga convergent margin. *Marine Geology*, **157**, 105–125.

Venturelli, G., Contini, S., Bonazzi, A., and Mangia, A. (1997) Weathering of ultramafic rocks and element mobility at Mt. Prinzera, Northern Apennines, Italy. *Mineralogical Magazine*, **61**, 765–778.

Ver Straeten, C.A. (2004) K-bentonites, volcanic ash preservation, and implications for Early to Middle Devonian volcanism in the Acadian orogen, eastern North America. *Geological Society of America*, **116**, 474–489.

Wang, W., Tang, J., Xu, W.-L., and Wang, F. (2015) Geochronology and geochemistry of Early Jurassic volcanic rocks in the Erguna Massif, northeast China: Petrogenesis and implications for the tectonic evolution of the Mongol-Okhotsk suture belt. *Lithos*, **218-219**, 73–86.

Whitney, D.L. and Evans, B.W. (2010) Abbreviations for names of rock-forming minerals. *American Mineralogist*, **95**, 185–187.

Wulaningsih, T., Humaida, H., Harijoko, A., and Watanabe, K. (2013) Major element and rare earth elements investigation of Merapi volcano, central Java, Indonesia. *Procedia Earth and Planetary Science*, **6**, 202–211.

Wright, V.P. and Tucker, M.E. (1991) *Calcretes*. Blackwell Scientific Publications, Oxford, 351 pp.

Yan, L.-L., He, Z.-Y., Jahn, B.-m., and Zhao, Z.-D. (2016) Formation of the Yandangshan volcanic-plutonic complex (SE China) by melt extraction and crystal accumulation. *Lithos*, **266-267**, 287–308.

Zaid, S.M. and Al Gahtani, F. (2015) Provenance, diagenesis, tectonic setting and geochemistry of Hawkesbury Sandstone (Middle Triassic), southern Sydney Basin, Australia. *Turkish Journal of Earth Sciences*, **24**, 72–98.

Zielinski, R.A. (1982) The mobility of uranium and other elements during alteration of rhyolite ash to montmorillonite: a case study in the Troublesome Formation, Colorado, U.S.A. *Chemical Geology*, **35**, 185–204.

Zhou, L., Zhang, Z., Li, Y., You, F., Wu,C., and Zheng, C. (2013) Geological and geochemical characteristics in the paleo-weathering crust sedimentary type REE deposits, western Guizhou, China. *Journal of Asian Earth Sciences*, **73**, 184–198.

(*Received 11 October 2016; revised 17 March 2017; Ms. 1142; AE: W.D. Huff*)